HHS Public Access

Author manuscript

Cell Rep. Author manuscript; available in PMC 2023 October 23.

Published in final edited form as:

Cell Rep. 2023 April 25; 42(4): 112371. doi:10.1016/j.celrep.2023.112371.

Connexin 43-mediated neurovascular interactions regulate neurogenesis in the adult brain subventricular zone

Nafiisha Genet[1,2,6,*], **Gael Genet**[1], **Nicholas W. Chavkin**[1], **Umadevi Paila**[1], **Jennifer S. Fang**[2,6], **Hema H. Vasavada**[1,2,6], **Joshua S. Goldberg**[2,6], **Bipul R. Acharya**[1], **Neha S. Bhatt**[2,3], **Kasey Baker**[2,3,4,5,6], **Stephanie P. McDonnell**[1], **Mahalia Huba**[1], **Danya Sankaranarayanan**[1], **Gerry Z.M. Ma**[7,8], **Anne Eichmann**[3,6], **Jean-Leon Thomas**[4,5,6], **Charles ffrench-Constant**[7,8], **Karen K. Hirschi**[1,2,6,9,*]

[1]Department of Cell Biology, Berne Cardiovascular Research Center, University of Virginia School of Medicine, Charlottesville, VA 22908, USA

[2]Departments of Medicine and Genetics, Yale University School of Medicine, New Haven, CT 06511, USA

[3]Department of Cellular and Molecular Physiology, Yale University School of Medicine, New Haven, CT 06511, USA

[4]Departments of Neuroscience and Cell Biology, Yale University School of Medicine, New Haven, CT 06511, USA

[5]Department of Neurology, Yale University School of Medicine, New Haven, CT 06511, USA

[6]Yale Cardiovascular Research Center, Yale University School of Medicine, New Haven, CT 06511, USA

[7]MRC Centre for Regenerative Medicine, University of Edinburgh, Edinburgh, UK

[8]Faculty of Medicine and Health Sciences, University of East Anglia, Norwich, UK

[9]Lead contact

SUMMARY

The subventricular zone (SVZ) is the largest neural stem cell (NSC) niche in the adult brain; herein, the blood-brain barrier is leaky, allowing direct interactions between NSCs and endothelial cells (ECs). Mechanisms by which direct NSC-EC interactions in the adult SVZ control NSC behavior are unclear. We found that Cx43 is highly expressed by SVZ NSCs and ECs, and

*Correspondence: nbg6s@virginia.edu (N.G.), kkh4yy@virgina.edu (K.K.H.).

AUTHOR CONTRIBUTIONS

N.G., G.G., N.W.C., J.S.F., H.H.V., J.S.G., B.R.A., N.S.B., K.B., and G.Z.M.M., performed experiments. S.P.M., M.H., and D.S. maintained mouse lines and performed mouse genotyping. U.P. and N.W.C. analyzed single-cell RNA sequencing data. B.R.A generated Cx43 lentiviral constructs. N.G., G.G., and K.K.H. designed experiments, analyzed data, and wrote the manuscript. A.E., J.-L.T., and C.ff.-C contributed to experimental design and manuscript editing.

DECLARATION OF INTERESTS

The authors declare no competing interests.

SUPPLEMENTAL INFORMATION

Supplemental information can be found online at https://doi.org/10.1016/j.celrep.2023.112371.

its deletion in either leads to increased NSC proliferation and neuroblast generation, suggesting that Cx43-mediated NSC-EC interactions maintain NSC quiescence. This is further supported by single-cell RNA sequencing and *in vitro* studies showing that ECs control NSC proliferation by regulating expression of genes associated with NSC quiescence and/or activation in a Cx43-dependent manner. Cx43 mediates these effects in a channel-independent manner involving its cytoplasmic tail and ERK activation. Such insights inform adult NSC regulation and maintenance aimed at stem cell therapies for neurodegenerative disorders.

In brief

In this study, Genet et al. describe the role of the gap junction protein connexin 43 in the adult brain subventricular zone where neural stem cells (NSCs) reside. Genet al. show that vascular endothelial cell-expressed connexin 43 is an important regulator of adult NSC proliferation and differentiation.

Graphical Abstract

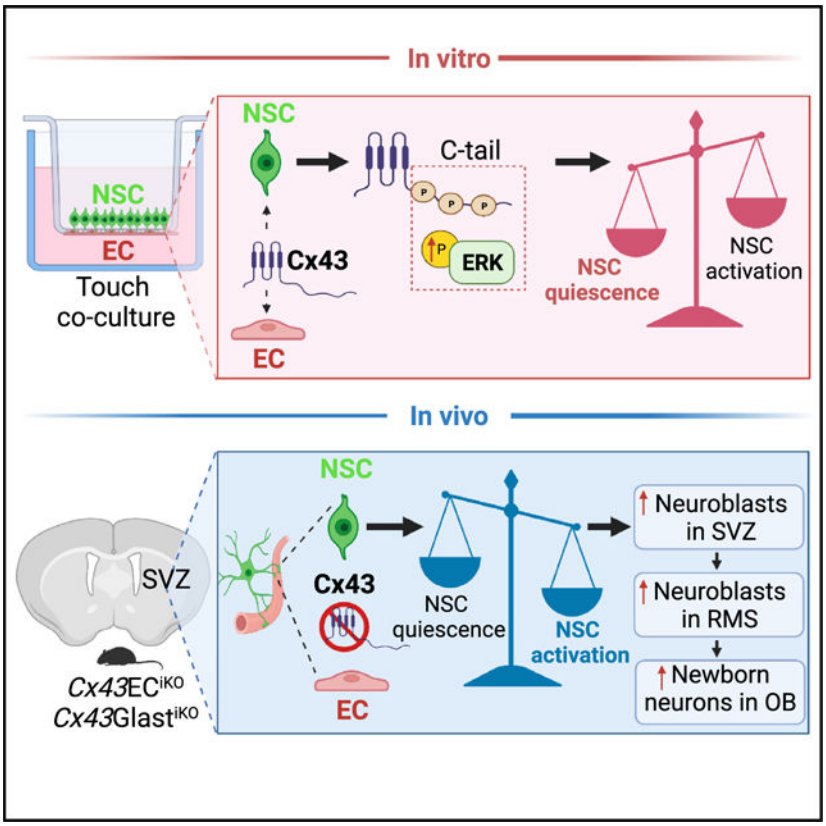

INTRODUCTION

In the adult mouse and human brains, neural stem cells (NSCs) reside in two germinal niches, the dentate gyrus of the hippocampus, or subgranular zone (SGZ), and the subventricular zone (SVZ) of the lateral ventricles, which is the largest NSC niche. In mice, both niches allow the replenishment of new neurons throughout life; the SGZ is involved

in hippocampal neurogenesis, while the SVZ enables olfactory bulb (OB) neurogenesis. The SVZ is a polarized niche, where neurogenesis is initiated when glial fibrillary acidic protein ($GFAP^+$) quiescent NSCs (qNSCs) are activated and become epidermal growth factor receptor ($EGFR^+$) NSCs that give rise to mammalian achaete-shute homolog 1 ($Mash\text{-}1^+$) transit-amplifying progenitor cells (TACs).[1–4] On the ventricular side of the murine SVZ, qNSCs protrude apical processes with short primary cilia that contact the ependymal cell layer lining the ventricles and cerebrospinal fluid within the ventricles.[1,5,6] On the parenchymal side, qNSCs project long basal endfeet that make direct contact with blood vessels in the niche.[7]

In the SVZ, TACs assemble into small clusters and differentiate into chains of doublecortin (DCX^+) neuroblasts[8]; TACs are fast dividing, while neuroblasts proliferate ten times slower.[2,6,9,10] The chains of neuroblasts, along with some clusters of TACs, migrate tangentially from the SVZ through a restricted pathway called the rostral migratory stream (RMS) toward their destination in the OB.[2,11] Once in the OB, neuroblasts exit the RMS and migrate radially into the granular and periglomerular layers to differentiate into interneurons.[9,12–14] In the adult SVZ, NSCs predominantly undergo symmetric, differentiative, and consuming divisions to generate TACs, which gradually depletes the pool of qNSCs over time.[15,16] Therefore, it is important to understand the signaling cues between NSCs and the other SVZ niche cells, especially vascular endothelial cells (ECs), to tightly regulate NSC activation, differentiation, migration, and neurogenesis.

It is well established that the SVZ microvascular ECs are fundamental to the niche and support NSC self-renewal, maintenance, proliferation, differentiation, and migration of neural progenitor cells (NPCs).[17,18] Several studies have highlighted the role of paracrine signaling between vascular ECs and NSCs in the SVZ via EC-secreted factors, such as vascular endothelial growth factor (VEGF)-A and VEGF-C,[19,20] betacelluline,[21] pigment epithelium-derived factor (PEDF),[22] and placental growth factor (PlGF) type 2,[23] that regulate NSC behavior in the SVZ. Moreover, in the SVZ microvasculature, and unlike other areas of the brain, the ECs that form the blood vessels lack pericyte and astrocyte coverage, enabling direct contact between NSCs and ECs in this niche.[18,24,25] This allows physical interactions between NSCs and ECs to enable juxtacrine signaling via membrane-bound proteins and their associated ligands enabling Notch and Ephrin signaling.[25,26] Intercellular junctions, such as gap junctions, also form between NSCs and ECs.[27] Gap junctions enable intercellular signaling via the transfer of ions, metabolites, soluble factors, and molecules of ≤1 kDa. In the developing mouse brain, gap junction proteins connexin 43 (Cx43) and Cx26 are differentially expressed and play important roles in the regulation of neurogenesis.[28,29] Gap junctions composed of Cx43 are known to form between NSCs and ECs in the mouse SVZ and RMS at various postnatal stages.[27] However, the role of EC- or NSC-expressed Cx43 in the regulation of adult SVZ neurogenesis is not known and is the focus of this study.

Herein, using an *in vitro* Transwell co-culture system, we showed that Cx43-mediated interactions between NSCs and ECs decrease NSC proliferation and increase their survival. Furthermore, in adult mice in which *Gja1*, which encodes for Cx43 protein, has been conditionally deleted in either NSCs or ECs for 1 week, there is an initial increase in NSC activation and the generation of DCX^+ neuroblasts. However, after 4 weeks' deletion, there

is a significant reduction of qNSCs in the SVZ and increased neurogenesis in the OB. Finally, we show that deletion of *Gja1* in ECs impairs the repopulation of the SVZ niche upon infusion of the antimitotic drug cytosine-β-arabinofuranoside (Ara-C). Collectively, these studies suggest that Cx43-mediated interactions between NSCs and ECs maintain NSC quiescence in a channel-independent manner involving ERK signaling to regulate neurogenesis in the adult SVZ. Such insights can be applied to the development of *ex vivo* biomimetic engineered SVZ niches to further study NSC regulation and to potentially use them to treat neurovascular disorders such as stroke.

RESULTS

NSC-EC co-culture decreases NSC proliferation in a Cx43-dependent manner

To investigate the effects of ECs on NSC behavior, we used a two-dimensional (2D) Transwell system in which ECs were co-cultured in contact with NSCs, allowing direct cell-to-cell interactions (Figures 1A and 1B). In this co-culture model, we used the commercially available bEnd.3 cells (American Type Culture Collection [ATCC]) as ECs and ANS4-GFP as NSCs. The ANS4-GFP cells are known to be representative of adult NSCs in the SVZ, as they express genes enriched in adult NSCs and are capable of differentiating into neurons and astrocytes when subjected to a permissive differentiation environment.[30] NSCs were seeded in the absence of epidermal growth factor (EGF) and fibroblast growth factor (FGF) (the growth factors that support NSC survival and growth) to specifically assess the role of ECs in the regulation of NSC behavior. We observed that ECs promote NSC survival, while NSC proliferation measured via EdU incorporation is significantly decreased (Figures 1C and 1D). Bulk mRNA sequencing (RNA-seq) of NSCs in co-culture with ECs revealed that genes associated with NSC quiescence, such as *Gfap*, *Sox9*, and *Prom1*, are upregulated, while genes associated with NSC activation, such as *Egfr* and *Ccne1*, are downregulated in comparison with NSCs cultured alone (Figure 1E). Gene Ontology (GO) analysis revealed that genes associated with neurogenesis are downregulated in NSCs when co-cultured with ECs (Figure 1F). Additionally, qPCR analysis performed on NSCs co-cultured with ECs showed increased mRNA levels of *Gfap*, *Nestin*, and *Glast*, genes associated with NSC quiescence, while expression of *Egfr*, *Mash1*, and *Cyclin E*, genes associated with NSC activation, is decreased (Figure 1G). Interestingly, these effects were not observed in in non-contacting co-culture conditions, suggesting that they are not mediated by soluble factors secreted by ECs (Figure S1A).

The RNA-seq analysis also revealed the upregulation of potential regulators of NSC-EC interactions (Figure 1E), including *Gja1* (also referred to as *Cx43*), which encodes the gap junction protein Cx43. This was of interest to us, as we previously found that Cx43 mediates interactions between ECs and vascular mural cells.[31] Thus, we used qPCR analysis to confirm that *Cx43* expression is increased in NSCs when co-cultured with ECs (Figure 1H). To determine whether Cx43 plays a role in mediating NSC-EC interactions that lead to changes in NSC gene expression, we used small interfering RNA (siRNA) to suppress *Cx43* expression in ECs and then co-cultured them with NSCs. This resulted in significantly decreased *Gfap* and *Glast* mRNA levels and significantly upregulated *Egfr*, *Mash1*, and *Cyclin E* mRNA levels (Figure 1I). Conversely, when we silenced *Cx43* in NSCs and then

co-cultured them with ECs, we did not observe changes in NSC genes expressions (Figures S1B–S1F). Collectively, these results suggest that ECs may enhance NSC survival and quiescence in Cx43-dependent manner.

ECs and NSCs in the adult brain SVZ highly express Cx43

In our RNA-seq studies, we found that *Gja1/Cx43* was the only gap junction gene significantly upregulated in NSCs when co-cultured with ECs (Figure 1E); however, both cell types have been shown to express other Cx proteins.[32,33] Thus, we measured the expression of different Cx proteins in ECs and NSCs *in vivo* in the adult mouse brain SVZ. Using immunohistochemistry and antibodies against different Cx proteins and CD31, which is expressed by all ECs, we found a low percentage of ECs expressing Cx26 and Cx31, while a high percentage of ECs express Cx43 (Figure 2A). To evaluate the expression of Cx proteins in NSCs in the murine SVZ, we first labeled the NSCs using a BrdU-labeling protocol in which label-retaining cells (LRCs) represent qNSCs.[34] We found that a percentage of SVZ LRC-NSCs express multiple Cx proteins, and a higher percentage of LRC-NSCs express Cx43 (Figure 2B), like ECs. To determine whether Cx43 is present between NSCs and ECs in the SVZ *in vivo*, we performed immunohistochemistry and high-resolution confocal imaging of SVZ coronal sections. We found punctate-like Cx43 expression between $CD31^+$ ECs and $GFAP^+SOX2^+$ NSCs, as well as between $SOX2^+$ cells of the ependymal layer (Figure 2C).

To determine whether NSC- and/or EC-expressed Cx43 plays a role in the regulation of NSCs in the adult brain SVZ, we used $Gja1^{flox/flox}$ mice (hereafter referred to as $Cx43^{fl/fl}$ mice) and an inducible loss-of-function genetic approach. To selectively delete *Cx43* in ECs, we crossed $Cx43^{fl/fl}$ with $Cdh5Cre^{iERT2}$ to generate *Cx43*EC^{iKO} mice, and to selectively delete *Cx43* in NSCs, we crossed $Cx43^{fl/fl}$ mice with $GlastCre^{iERT2}$ to generate *Cx43*$Glast^{iKO}$ mice. To validate Cre-mediated recombination in ECs and NSCs in these models, we crossed both *Cx43*EC^{iKO} and *Cx43*$Glast^{iKO}$ mice with $ROSA^{mT/mG}$ mice in which, upon tamoxifen (Tx) injection, cell membrane-localized tdTomato converts to GFP in Cre recombinase-expressing cells. We performed recombination and genetic deletion in 6-week-old young adult mice with Tx injection, as shown in the timeline in Figure 2D. As expected, we observed GFP^+ ECs in the SVZ of *Cx43*EC^{iKO};$ROSA^{mT/mG}$ mice and GFP^+ NSCs in the SVZ of *Cx43*$Glast^{iKO}$;$ROSA^{mT/mG}$ (Figure 2E).

To further confirm the loss of Cx43 expression in our mouse models, we also performed immunostaining with antibodies against CD31 to label ECs and antibodies against SOX2 and GFAP to co-label NSCs. In the SVZ of *Cx43*EC^{iKO} mice, we found loss of Cx43 expression in the $CD31^+$ ECs and maintenance of Cx43 expression in ependymal cells and NSCs. In the SVZ of *Cx43*$Glast^{iKO}$ mice, we found Cx43 expression was lost in $GFAP^+SOX2^+$ NSCs, while ECs and ependymal cells retained expression (Figure 2F). *Cx43* deletion efficiency in ECs of *Cx43*EC^{iKO} and NSCs of *Cx43*$Glast^{iKO}$ was confirmed via qPCR analysis of primary SVZ cells dissociated and isolated into EC ($CD31^+CD45^-Glast^-$) and NSC ($Glast^+CD45^-CD31^-$) fractions using fluorescence-activated cell sorting (FACS) (Figure S2). Our studies showed that in *Cx43*EC^{iKO} mice, ECs lost ~90% of *Cx43* expression, which was maintained in NSCs. Conversely, in *Cx43*$Glast^{iKO}$ mice, *Cx43*

expression was suppressed by ~75% in NSCs and maintained in ECs (Figure 2G). These results demonstrate effective deletion of Cx43 in SVZ ECs and NSCs in Tx-induced *Cx43*EC^{iKO} and *Cx43*Glast^{iKO} mice, respectively.

Cx43 deletion in ECs or NSCs depletes qNSCs in the adult SVZ

We next analyzed the consequences of short-term (1 week post-Tx) and long-term (4 weeks post-Tx) deletion of *Cx43* in *Cx43*EC^{iKO} and *Cx43*Glast^{iKO} mice, compared with control *Cx43*$^{fl/fl}$, on the number of qNSCs and activated NSCs (aNSCs) and neuroblasts in the adult SVZ (Figures 3A and 3B). The identification of qNSCs is a challenge because of the lack of specific markers. In our study, we used combined expression of the astrocytic marker GFAP and the neural stem and progenitor cell marker SOX2 to identify NSCs.[25,35,36] As SOX2 and GFAP are expressed by both qNSCs and aNSCs,[18] we injected *Cx43*EC^{iKO} and *Cx43*Glast^{iKO} mice, at 1 and 4 weeks post-Tx, with EdU 24 h prior to sacrifice to measure qNSCs (EdU^{-}) and aNSCs (EdU^{+}).

At 1 week post-*Cx43* deletion, we observed a decrease in the number of GFAP^{+}SOX2^{+}EdU^{-} qNSCs in both *Cx43*EC^{iKO} and *Cx43*Glast^{iKO} SVZ (Figures 3C and 3I) and further reduction at 4 weeks post-Tx (Figures 3F and 3I). Additionally, the absence of GFAP^{+} cells co-expressing S100β in the striatum of the mutant SVZs shows that the decrease in qNSCs observed at 4 weeks post-*Cx43* deletion is not due to abnormal astrogliosis (Figure S3A). We also observed significantly increased EGFR^{+}SOX2^{+}EdU^{+} aNSCs in both mutant SVZs at 1 week post-Tx (Figures 3D and 3J); however, at 4 weeks post-Tx, the number of aNSCs was significantly decreased (Figures 3G and 3J). Neuroblasts, identified via expression of DCX, were significantly increased in both *Cx43*EC^{iKO} and *Cx43*Glast^{iKO} SVZ at 1 week post-*Cx43* deletion (Figures 3E and 3K), while their number was significantly reduced in both mutants at 4 weeks post-Tx (Figures 3H and 3K). Furthermore, we used *Cx43*Glast^{iKO};ROSA$^{mT/mG}$ mice to perform lineage tracing at 1 week post-*Cx43* deletion. We found DCX^{+} neuroblasts (Figure S3B, white arrowheads) localized within the recombinant GFP^{+} population, supporting that the neuroblasts generated in the *Cx43*Glast^{iKO} SVZ (Figures 3E and 3K) were derived from *Cx43*-deficient NSCs.

Elsewhere in the brain, with exception of the SVZ, vascular ECs interact with astrocytes and pericytes via Cx43, which promotes their blood-brain barrier (BBB) function.[37–39] Thus, we sought to determine whether deletion of *Cx43* in vascular ECs or Glast-expressing astroglial cells compromised BBB integrity and caused vascular leakage. To assess vascular permeability, we injected *Cx43*$^{fl/fl}$, *Cx43*EC^{iKO}, and *Cx43*Glast^{iKO} mice with 2% Evans blue 24 h prior to sacrifice, as depicted in Figure S4A, and evaluated vascular leakage in brain and liver tissues. As expected, we did not observe vascular leakage in the control brains; there was also no leakage in the mutant brains (Figure S4B). In contrast, in liver tissues that lack barrier function, leakage of Evans blue dye from the vasculature was evident throughout control and mutant tissues (Figure S4C). In addition, using Vascupaint green perfusion, we did not observe any differences in *Cx43*EC^{iKO} and *Cx43*Glast^{iKO} brain microvasculature morphology at 4 weeks post-Tx, compared with *Cx43*$^{fl/fl}$ controls (Figures S4D and S4E). Thus, deletion of *Cx43* in vascular ECs or astroglial cells does not appear to compromise BBB integrity in the adult brain. We also measured brain and OB areas

and found no differences between *Cx43*$^{fl/fl}$ control mice and *Cx43*EC^{iKO} and *Cx43*Glast^{iKO} mice after short- or long-term deletion of *Cx43* (Figure S5).

Single-cell RNA sequencing analysis of ECs and NSPCs isolated from Cx43EC^{iKO} and Cx43Glast^{iKO} SVZs

To gain a deeper understanding of the Cx43-dependent molecular regulation of NSC behavior, we employed a single-cell RNA sequencing (scRNA-seq) approach. We dissected the lateral walls of the lateral ventricles of *Cx43*$^{fl/fl}$, *Cx43*EC^{iKO}, and *Cx43*Glast^{iKO} mice at 1 week post-Tx (Figure 4A). After microdissection, we dissociated the SVZ cells and FACS-isolated ECs (CD31^{+}Glast^{-}CD45^{-}) and neural stem and progenitor cells (NSPCs; CD31^{-}Glast^{+}CD45^{-}) that were used for scRNA-seq analysis. After filtering, samples (2,159 cells for *Cx43*$^{fl/fl}$, 3,242 for *Cx43*EC^{iKO}, and 2,029 for *Cx43*Glast^{iKO}) were processed for single cell barcoding and downstream mRNA library preparation and sequencing (Figure 4B). Relative RNA expression of known marker genes associated with qNSCs, aNSCs, and NPCs (i.e., transit-amplifying progenitor cells and neuroblasts), as well as ECs and astrocytes, were used to annotate the 5 populations.[40–43] More specifically, cells exhibiting high relative mRNA expression of (1) *Gfap*, *Sox2*, and *Prom1* are qNSCs; (2) *Egfr* are aNSCs; (3) *Ascl1*, *Mki67*, *Dcx*, *Sox4*, *Sox11*, and *Ccnd2* are NPCs; (4) *Pecam1* are ECs; and (5) *S100β* are astrocytes (Figures 4C and 4D). To further support the results presented in Figure 3, we show at the single-cell level that mRNA expression of genes enriched for neuroblast identity, including *Sox4*, *Sox11*, and *Dcx*, are upregulated in the NPCs isolated from the SVZ of *Cx43*EC^{iKO} and *Cx43*Glast^{iKO} mice (Figure 4E). These results support that absence of *Cx43* expression in either ECs or NSCs upregulates the expression of genes enriched for neuroblast identity.

Cx43 deletion in ECs or NSCs increases neuroblast generation in the RMS and neurogenesis in the OB

As neuroblasts generated in the SVZ migrate toward the OB via the RMS, we next assessed whether increased neuroblast generation in the *Cx43*EC^{iKO} and *Cx43*Glast^{iKO} SVZs at 1 week post-Tx leads to increased neuroblasts in the RMS (Figure 5A). On brain sagittal sections immuno-stained with anti-DCX, we analyzed the anterior portion of the RMS recognized by its elbow-shaped morphology (Figures 5B and 5C). In this region, we found significantly increased DCX^{+} neuroblasts in *Cx43*EC^{iKO} and *Cx43*Glast^{iKO} mice, compared with *Cx43*$^{fl/fl}$ controls (Figures 5D and 5E). We next examined whether the observed increase in neuroblasts in *Cx43*EC^{iKO} and *Cx43*Glast^{iKO} RMS at 1 week post-Tx affects neurogenesis in the OB. To do so, we used a LRC protocol (Figure 5F), in which 6-week-old young adult mice received 3 consecutive EdU injections on the first 3 days of a 5 day Tx induction. At 4 weeks post-Tx, mice were analyzed using immunostaining with anti-EdU and anti-NeuN, to label newborn neurons.[2,44] Interestingly, we observed a significantly increased number of LRC/NeuN^{+} interneurons in the granule cell layer (GCL) of both *Cx43*EC^{iKO} and *Cx43*Glast^{iKO} OB compared with *Cx43*$^{fl/fl}$ controls (Figures 5G–5I).

To determine whether neurons in the *Cx43*Glast^{iKO} RMS were derived from SVZ NSCs, we used *Cx43*Glast^{iKO};ROSA$^{mT/mG}$ mice to perform lineage-tracing studies (Figure S6A). We found LRC/NeuN^{+} cells (Figure S6B, white arrows) localized within the recombinant GFP^{+}

population, supporting that the newborn olfactory neurons generated in the *Cx43*Glast^{iKO} SVZ (Figures 3E and 3K) were derived from *Cx43*-deficient NSCs. Importantly, the increase in newborn neurons in *Cx43*EC^{iKO} and *Cx43*Glast^{iKO} OB was not a consequence of neuronal death, as we did not observe changes in apoptosis levels in *Cx43*EC^{iKO} and *Cx43*Glast^{iKO} OB measured via immuno-staining for cleaved CASPASE-3 (Figures S6C–S6E). Collectively, these results suggest that the short-term deletion of *Cx43* in ECs or NSCs leads to decreased qNSCs and increased aNSCs in the SVZ, as well as increased neuroblast generation in the SVZ and RMS. After long-term deletion of EC- or NSC-expressed *Cx43*, the qNSC pool in the SVZ is further depleted, while aNSCs and neuroblasts are exhausted from the SVZ, and neurogenesis is increased in the OB. Thus, both EC- and NSC-expressed Cx43 contribute to the regulation of adult SVZ neurogenesis.

EC-expressed Cx43 is necessary for SVZ niche repopulation

Our studies suggested that NSC quiescence and maintenance in the SVZ niche is regulated by ECs in a Cx43-dependent manner. Thus, we tested whether lack of EC-expressed Cx43 would impair NSC-mediated SVZ niche repopulation after depletion of all SVZ proliferating cells (aNSCs, TACs, and neuroblasts) via the antimitotic drug Ara-C (cytosine-β-D-arabinoside). At 1 week post-Tx injections in *Cx43*EC^{iKO} and *Cx43*$^{fl/fl}$ control mice, Ara-C (2%) or saline (control) was infused directly in one of the two lateral ventricles (ipsilateral) via a cannula connected to a subcutaneously implanted micro-osmotic pump for 6 consecutive days (Figures 6A and 6B). EdU was administered to label actively proliferating cells 24 h prior to sacrifice. The intracerebroventricular injection coordinates were verified via injection of 1% Fast Green dye, as previously described[45] (Figure S7).

We first confirmed that Ara-C treatment depleted all EdU^{+} proliferating cells (Figures 6C and 6D), as well as DCX^{+} neuroblasts (Figures 6E and 6F), in the SVZ. Importantly, we observed increased DCX^{+} neuroblasts in control, saline-infused *Cx43*EC^{iKO} SVZ compared with *Cx43*$^{fl/fl}$ (Figures 6E and 6F). These results are consistent with data shown in Figure 3K, which demonstrates that short-term deletion of *Cx43* in *Cx43*EC^{iKO} leads to increased SVZ neuroblasts. Subsequently, we analyzed the number of DCX^{+} neuroblasts in the SVZ 6 days after saline or Ara-C withdrawal (Figure 6G, chase period). DCX^{+} neuroblasts were significantly reduced in saline-treated *Cx43*EC^{iKO} SVZ, compared with *Cx43*$^{fl/fl}$ (Figures 6H and 6I), which is also consistent with Figure 3K that shows reduced DCX^{+} neuroblasts after long-term deletion of *Cx43* in *Cx43*EC^{iKO} SVZ. In addition, we found that DCX^{+} neuroblast repopulation in Ara-C-treated *Cx43*EC^{iKO} SVZ is significantly reduced compared with Ara-C-treated *Cx43*$^{fl/fl}$ SVZ (Figures 6H and 6I). Thus, absence of *Cx43* in ECs impairs the repopulation of the SVZ niche post-Ara-C treatment, further supporting that Cx43 expression in ECs contributes to the maintenance of the qNSC pool in the SVZ and prevents their premature activation and depletion.

Cx43 cytoplasmic tail mediates EC-induced NSC quiescence in an ERK-dependent manner

We next investigated the mechanism(s) by which *Cx43* regulates NSC-EC interactions to maintain NSC quiescence. Cx43 can function in a channel-dependent or channel-independent manner; thus, we created lentiviral constructs to express Cx43 mutant proteins to perform structure-function studies to determine how Cx43 mediates NSC-EC interactions.

To investigate channel-dependent functions, we generated a Cx43 channel-dead mutant (*Cx43T154A*) that allows gap junction channel formation but blocks Cx43 channel activity.[46] To investigate channel-independent functions, we generated mutant Cx43 that lacks its cytoplasmic tail (*Cx43CTΔ258*),[47] which can mediate intracellular signaling, independent of channel formation.[48] ECs and NSCs were treated with si*Cx43* to suppress endogenous Cx43 expression, and then transduced with lentiviral constructs to express the mutant Cx43 proteins. Expression of the Cx43 cytoplasmic tail truncated mutant (*Cx43CTΔ258*, 1 μg) led to a significant downregulation of genes associated with NSC quiescence (*Gfap*, *Nestin*, and *Glast*), while expression of the Cx43 dead-channel mutant (*Cx43T154A*, 0.5 μg) had no effect on NSC gene expression (Figures 7A, S8A, and S8B). Additionally, when we treated both NSCs and ECs with ^{43}gap 26 peptide (100 nM), which blocks Cx43 channel activity, we did not observe any changes in NSC gene expression associated with either quiescence or activation (Figure 7B). Thus, it appears that EC-mediated NSC quiescence is regulated by *Cx43* in a channel-independent manner. We assessed whether overexpression of *Cx43* in NSCs alone was sufficient to suppress NSC proliferation, as measured via EdU incorporation, and found that Cx43 overexpression in NSCs does not affect their proliferation (Figures S8C–S8G).

It is known that the Cx43 cytoplasmic tail is involved in the activation of downstream effectors involved in ERK signaling,[48,49] and interestingly, we observed increased ERK activation in NSCs when co-cultured with ECs and the latter is abrogated in NSCs co-cultured with ECs silenced for *Cx43* (Figures 7C and 7D). Furthermore, inhibition of ERK signaling with U0126 (10 μM) in NSCs co-cultured with ECs abolished the effect of ECs on NSC expression of genes associated with quiescence (Figure 7E). Finally, the scRNA-seq analysis of NPCs isolated from SVZs of *Cx43*$^{fl/fl}$, *Cx43*EC^{iKO}, and *Cx43*Glast^{iKO} mice revealed that the expression of genes known to be directly induced downstream of the ERK/MAPK signaling pathway (i.e. *Jun*, *Fos*, *Ets1*, *Ccnd1*, *Sp1*, and *Myc*)[50] are downregulated in NPCs from both knockout (KO) models (Figure 7F), Interestingly, the scRNA-seq analysis also revealed decreased expression of several mRNAs encoding proteins known to directly interact with the cytoplasmic domain of Cx43, such as β-catenin and ZO-1,[51] in NPCs isolated from *Cx43*EC^{iKO} and *Cx43*Glast^{iKO} SVZ (Figure 7G). Collectively, our data support a role for the Cx43 cytoplasmic tail in the regulation of NSC quiescence via ERK activation. Our *in vitro* and *in vivo* findings are summarized in the graphical abstract.

DISCUSSION

NSCs in the adult brain SVZ reside in a vascularized niche, which is known to regulate their proliferation, migration, and differentiation via niche cell-derived secreted factors.[21,22,52–56] It is also well established that NSC basal endfeet are in direct contact with vascular ECs, allowing neuro-vascular interactions.[7] Little is known about the role of direct NSC-EC contact in the regulation of adult SVZ maintenance and neurogenesis. In these studies, we investigated the role of EC- and NSC-expressed Cx43 therein.

Cx43 is known to be expressed in both the embryonic and adult SVZ, where it maintains NSC survival, and can also either promote or arrest NPC proliferation.[27,57–60] That is, during embryonic brain development, Cx43 is required to maintain mouse cortical NPCs in

a proliferative state.[57] In contrast, in post-natal and adult neurogenesis, *Cx43* expression is increased in SVZ NPCs and is inversely correlated with their proliferation, as assessed using BrdU labeling.[57]

Our data are consistent with, and extend, these previous observations. We show that deletion of *Cx43* in either ECs or NSCs in the adult SVZ leads to increased NSC activation and depletion of the qNSC pool over time. This results in increased neuroblasts in the RMS and ultimately increased newborn neurons in the OB. Whether increased newborn neurons in the OB lead to functional neurons that fully integrate into the olfactory neuronal circuits and modifies olfactory function in these Cx43-deficient mice is not yet known.

We further show that ECs regulate NSC quiescence via ERK activation, in a Cx43-dependent manner. This result is consistent with a previous study showing that in the adult SVZ, ERK1/2 is activated only in qNSCs and, in the aged SVZ, there is reduced pERK1/2 signaling, associated with depletion of the qNSC pool.[61] Whether Cx43 expression in the SVZ is reduced with aging and mediates age-related decreased ERK activation and NSC quiescence remains to be determined.

During embryonic brain development, the non-channel function of Cx43 directs neuronal migration via Cdk5 phosphorylation of its cytoplasmic tail.[62] Herein, we found that Cx43-mediated NSC quiescence in the adult brain is also dependent of its cytoplasmic tail, suggesting a channel-independent function. Over-expression of Cx43 in NSCs does not mimic the effects of EC-expressed Cx43 on NSC behavior or gene expression. Thus, although it is possible that, in NSCs, ERK signaling via the Cx43 cytoplasmic tail enables the activation of downstream effectors that promote NSC quiescence, the regulatory mechanisms are likely to be more complex. Nevertheless, we found that expression of *Ctnnb1* and *Tjp1*, genes encoding for β-catenin and ZO-1 proteins, respectively, are downregulated in NPCs isolated from *Cx43*EC^{iKO} and *Cx43*Glast^{iKO} SVZ. β-Catenin and ZO-1 are known to interact directly with the Cx43 cytoplasmic tail and activate MAPK/ERK signaling.[63,64] Further mechanistic studies are required to determine how Cx43, possibly via β-catenin/ZO-1 interactions, regulate ERK activation to promote NSC quiescence.

In the dentate gyrus of the hippocampus, the other neurogenic niche of the adult brain, Cx43 is thought to regulate neurogenesis in a channel-dependent manner.[65] However, unlike in our studies, in which we deleted *Cx43* in either ECs or NSCs with *Cdh5*Cre^{ERT2} and *Glast*Cre^{ERT2} mice, respectively, the previous study used *Nestin*Cre^{ERT2} mice crossed with *Cx43*$^{fl/fl}$G138R mice that express a point mutation in the cytoplasmic loop of Cx43 causing channel closure without affecting protein-protein interactions mediated by Cx43.[65] Furthermore, we performed additional mechanistic *in vitro* studies and scRNA-seq analysis that collectively support a non-channel function of Cx43 in the regulation of adult neurogenesis.

Interestingly, our *in vivo* results show the same outcome whether Cx43 is deleted in ECs or NSCs while, *in vitro*, only EC-expressed Cx43 mediates effects on NSC proliferation and survival. There are many differences between the two systems that can account for this finding, including lack of other SVZ components in NSC-EC co-cultures that may be

important for this regulation. In addition, in the *in vitro* studies, NSCs were silenced for *Cx43* prior to co-culture with ECs, while *in vivo* NSCs and ECs were in contact prior to *Cx43* deletion in either ECs or NSCs. Thus, there are likely more complex interactions between ECs and NSCs, and perhaps other cell types, in the SVZ niche that depend on EC- and NSC-expressed Cx43.

In summary, we used both *in vitro* and *in vivo* approaches to gain insight into the role of Cx43 in the regulation of NSCs in the adult SVZ. We show that EC- and NSC-expressed Cx43 is required to maintain NSC quiescence. Further mechanistic studies are needed to determine exactly how Cx43 regulates NSC behavior in the adult SVZ, and our *in vitro* studies suggest that this occurs in a channel-independent manner. Such insights can be applied to the bioengineering of a NSC niche *ex vivo* that better mimics its *in vivo* environment, to enable sustained NSC viability and functional properties aimed at stem cell therapies for neurological disorders.

Limitations of the study

In this study, we chose *Glast*Cre^{ERT2} instead of *Nestin*Cre^{ERT2} mice to specifically address the role of Cx43 in NSCs without affecting its expression in ependymal cells, where *Nestin* is also expressed.[1,66] We cannot rule out that the deletion of *Cx43* in *Cx43*Glast^{iKO} mice affects Cx43 expression in astrocytes outside the SVZ; however, importantly, we show preserved blood-brain barrier integrity in the *Cx43*Glast^{iKO} mice. Additionally, to further confirm our mechanistic findings, new mouse models that either lack the Cx43 cytoplasmic tail (CTΔ258) or are *Cx43* channel dead (*Cx43*T154A) would be needed.

STAR★METHODS

RESOURCE AVAILABILITY

Lead contact—Further information and requests for resources should be directed and will be fulfilled by the lead contact, Karen K. Hirschi (kkh4yy@virginia.edu).

Materials availability—All unique materials and reagents will be available upon request to the lead contact.

Data and code availability

- The single cell RNA seq data of SVZ populations have been deposited at Gene Expression Omnibus database (GEO) and are publicly available. The accession number for the dataset is listed in the key resources table.
- This paper does not report original code.
- Any additional information regarding the data reported in this work is available from the lead contact upon request.

EXPERIMENTAL MODEL AND SUBJECT DETAILS

Mice—Male and female mice were used to minimize gender-related biased results. All animal protocols and procedures were reviewed and approved by the University

of Virginia Animal Care and Use Committee (protocol #4277) and complied with all ethical regulations. *Cdh5*Cre^{ERT2}1Rha (also referred to as *VE-Cadherin*Cre^{ERT2})[67,68] and *GLAST*Cre^{ERT2} (*Slc1a3*Cre^{ERT2})[69] were gifts from Drs. Ralf Adams and Jean Lé on Thomas labs, respectively. *Gja1*$^{flox/flox}$ (also referred to as *Cx43*$^{flox/flox}$) and ROSA$^{mT/mG}$ mice were commercially purchased. For genetic loss-of-function studies, *Cdh5*Cre^{ERT2} and *GLAST*Cre^{ERT2} animals were crossed to mice carrying a loxP-flanked *Gja1* gene (*Cx43*$^{flox/flox}$) to create *Cx43*EC^{iKO} and *Cx43*Glast^{iKO}, respectively. Mice were maintained under standard pathogen-free conditions. To induce Cre activity in *Cx43*EC^{iKO} and *Cx43*Glast^{iKO}, 6-week-old young adult mice received intraperitoneal (i.p.) injections of Tamoxifen (Tx, 2mg/day) for 5 consecutive days, which resulted in ~90% and ~75% *Gja1* deletion in ECs of *Cx43*EC^{iKO} and NSCs of *Cx43*Glast^{iKO} respectively, as assessed by qPCR (Figure 3E). Tx-injected *Cx43*$^{flox/flox}$ littermates were used as controls. Mice were analyzed at: (1) 8-week-old after 1 week-post final Tx injections for short-term deletion studies and (2) at 11-week-old after 4 week-post final Tx injections for long-term deletion studies. For Ara-C studies, mice were analyzed at 2- and 3-week-post final Tx injection. To label actively proliferating progenitors in the SVZ, mice received an i.p. injection of EdU (50 mg/kg) 24 h prior to sacrifice. We used label retention to identify quiescent NSCs that are slow-cycling cells, also known as label retaining cells (LRC) that retain BrdU or EdU for extended periods due to their relatively long cycling times.[18,70,71] To do so, mice received 5 consecutive injections of BrdU or 3 consecutive EdU injections on the first 3 days of the 5 days of Tx injections, mice were analyzed 4-weeks post-Tx at 11-week-old. For Ara-C studies, the mice were 9-week-old for the depletion studies and 10-week-old for the chase studies at the time of analysis.

METHOD DETAILS

Mouse genotyping—Ear sample DNA was lysed using the hotshot method. Samples were lysed in alkaline lysis reagent (pH 12) containing 25mM NaOH and 0.2mM EDTA for 1 h at 90°C. Subsequently, samples were neutralized using 40mM Tris-HCl. PCR was performed in PCR-ready tubes (Bioneer Inc. K-2016) containing 1μL of DNA sample and 12.5 mM primers for a final reaction volume of 20μL adjusted with RNAse-free H_2O. PCR genotyping primers sequences are documented in Table S1.

FACS isolation of primary ECs and NSCPs from mouse brain cortex and SVZ —Brain cortex and SVZ were harvested (5 brains at a time to maximize cell viability), minced into small pieces of ~1 × 1 mm in size, then subjected to enzymatic dissociation in collagenase/dispase (Roche, 100 mg/ml stock) solution for 30 min at 37°C in a hybridization oven with constant rotation.[72] Subsequently, the digested tissues were triturated in 2% FBS in PBS supplemented with DNAse (10 mg/mL stock solution) with a P1000 pipette (~100x). Afterward, debris and myelin were removed with Percoll, cells were pelleted by centrifugation and resuspended in HBSS/BSA/glucose buffer for immunostaining. Antibodies (listed in key resources table) were added to the resuspended cells (1 μL of antibody/10^5 cells) and incubated during 20 min on ice protected from light. Post-immuno-staining cells were washed with HBSS/BSA/glucose buffer and filtered through a 40 μm cell strainer. Cells isolated from the cortex were used as unstained, single-color and FMO controls (each combination of all antibodies except one), as well as isotype controls to set up

gating and compensation strategy (Figure S2). From SVZ CD45^{-} cells, ECs (CD31^{+}Glast^{-} population) and NSPCs (Glast^{+}CD31^{-} population) were collected using a BD FACS Melody cell sorter equipped with a 100 μm nozzle in pre-filled FACS tubes with EC and NSC media respectively to cushion the cells. Post-FACS processing, cells are pelleted, snap frozen in liquid nitrogen and stored at −80°C for RNA isolation.

Library preparation and sequencing—FACS-purified live single cell suspensions were submitted to the University of Virginia Genome Analysis and Technology Core (RRID:SCR_018883) for single cell RNA library preparation and next-generation sequencing. Single cell RNA libraries were prepared using the 10X Genomics Chromium Next GEM Single Cell 3′ Reagent Kit v3.1 (PN-1000121) and Chromium Controller. Next-generation sequencing was performed using an Illumina NextSeq 2000 Sequencing System on the P3 flow cell with a 100 bp paired-end sequencing reagent kit. Two biological replicate samples for each condition were prepared, sequenced, and aligned using CellRanger v5.0.0 to the mm10 genome. Estimated cell number outputs for each sample were: *Cx43*$^{fl/fl}$ (1) = 1083; *Cx43*$^{fl/fl}$ (2) = 1076; *Cx43*Glast^{iKO} (1) = 710; *Cx43*Glast^{iKO} (2) = 1319; *Cx43*EC^{iKO} (1) = 571; *Cx43*EC^{iKO} (2) = 2674. Sequencing yielded a mean of ~70,000,000 reads/sample, ~78,000 reads/cell, and ~1,500 genes/cell.

Processing and analysis of single cell RNAseq data—Filtered feature-barcode matrices generated by CellRanger were further processed using version 4.2 of the Seurat package (PMCID: PMC8238499) in R. The single cell data for each sample was filtered to include features detected in at least 3 cells and cells were selected that had at least 200 features expressed. After performing QC metrics guided by plots, we further eliminated some cells to account for possible dying or dead cells and doublets. We also excluded cells with more than 10–25% of the transcripts coming from mitochondrial genes. An improved method based on regularized negative binomial regression “sctransform” (PMCID: PMC6927181) was used for normalization of the data. We performed data integration using methods for finding anchors across the datasets (i.e., 2 *Cx43*$^{fl/fl}$, 2 *Cx43*EC^{iKO} and 2 *Cx43*Glast^{iKO} that ensured a comparative analysis across the three experimental conditions. An integrated downstream analysis of all cells was performed with Seurat using FindNeighbors and FindClusters functionality and UMAP was used for dimensionality reduction. For all downstream marker analysis, we used the normalized “RNA assay” for the identification of cell populations and for comparisons across the three experimental conditions.

Tissue collection, subventricular zone (SVZ), rostral migratory stream (RMS) and OB immunohistochemistry and imaging—Mice were sacrificed with a lethal dose of ketamine (80 mg/kg body weight)/xylazine (8 mg/kg body weight). Mice received trans-cardiac infusion of 10mL sterile PBS supplemented with 2mM EDTA and 10U/mL heparin followed by 10mL 3.7% formaldehyde. Brain tissues were post-fixed with 3.7% formaldehyde at 4°C overnight. Post-fixation, brains were washed 3 times during 30 min in PBS 1X. SVZ coronal sections, sagittal sections of the RMS and coronal sections of the OB were collected in a 24-well plate in a sequential manner and subsequently subjected to a free-floating slice immunostaining protocol. All sections were cut at 50 μm

with a Leica vibratome (VT1000S). Briefly, slices were permeabilized with 0.5% Triton X-100 for 30 min at room temperature (RT). If EdU staining was required, we proceeded with EdU staining post-permeabilization following the manufacturer's protocol (Click-iT – ThermoFisher C10337). Sections were then blocked with 10% donkey serum in PBS 1X supplemented with 0.3% Triton X-100 (blocking buffer) for 1 h at RT. After blocking, sections were incubated with appropriate primary antibodies (listed in Table S2) diluted in blocking buffer overnight at 4°C, on a low-speed rocking plate. Samples were washed three times with PBS 1X supplemented with 0.1% Triton X-100 (PBST) then incubated with respective conjugated secondary antibodies for 1 h at RT. After 3 washes with PBST, Hoechst (4 μM) was added during 30 min for nucleus counterstaining. SVZ images were acquired with an inverted Leica SP8 DMi8 high-resolution confocal microscope equipped with adaptive deconvolution (LIGHTNING, Leica) using 63x or 203 objectives. A series of 3–5 SVZ slices from each animal taken from the same rostro-caudal area, judged by the shape of the lateral ventricles, of the corpus callosum and the anterior commissure were imaged. We localized the RMS attached to the OB between a sagittal depth of 3.2–3.35mm from the lateral side of the brain toward the midline. For OB analysis, the whole OB was cut coronally. Images were post-analyzed using ImageJ and Photoshop (Adobe) software.

Evans blue permeability assay—To assess changes in vascular permeability, mice received an i.p. injection of 2% Evans blue and were sacrificed 24 h later. Prior to brain and liver harvesting, mice were infused with PBS 1X supplemented with 2mM EDTA and 10U/mL heparin to wash out any traces of blood and maintain vessel integrity. Brains were post-fixed in 3.7% formaldehyde overnight and imaged using a dissecting microscope equipped with a digital camera (Leica).

Vascupaint silicone rubber injection—To assess changes in the brain microvaculature, mice were injected with 4 mL of Vascupaint (green) following the manufacturer's protocol (ediLumine, SKU MDL-122). Post-vascupaint injection, brains were harvested and post-fixed in 3.7% formaldehyde overnight. Brains were then dehydrated with 30%, 60% and 100% methanol successively for 24h each. Post-dehydration, brains were clarified with 1:1 of Benzyl Benzoate (Cat #B6630–1L):Benzyl alcohol (Cat # 305197–1L) for 48h and imaged using a Nikon SMZ-745T Trinocular 4K Digital Stereo microscope.

Ara-C infusions—2% Cytosine-β-D-arabinofuranoside or Ara-C (Sigma) in saline or saline alone was infused directly in one of the two lateral ventricles (ipsilateral side) of adult mice (8-week-old) via a cannula (Alzet brain infusion kit 3) implanted stereotaxically in a 1mm burr hole drilled on the surface of the brain at the following coordinates: 1.4 mm lateral and 0.5 mm rostral to bregma.[6,73] Intracerebroventricular injection coordinates were verified with the injection of Fast Green dye 1%[45] (Figure S7). The cannula was connected to a subcutaneously implanted micro-osmotic pump (Alzet model 1007D flow rate 0.5 μl/h, 7 days). After 6 days of infusion, the pump was removed, and mice were sacrificed at the indicated survivals. The success of the Ara-C infusion was evaluated by immunostaining for the neuroblast marker, DCX and the proliferation marker EdU.

RNA isolation—RNA from primary ECs and NSCs, as well as bEnd.3 and ANS4-GFP cells, were purified using RNeasy Plus micro kit (Qiagen). 1 μg of RNA was reverse transcribed using high-capacity cDNA Reverse transcription kit (Applied Biosystems). Quantitative PCR was performed on 15 ng cDNA using PowerUp SYBR Green Master Mix (Applied Biosystems) and the corresponding primers (supplementary Materials and Methods Table S2). The data were first normalized to actin level in each sample, and the relative expression levels of different genes were calculated by the comparative Ct method.[74]

siRNA transfection—*Cx43* siRNA (Smartpool siRNA *Cx43*, L-051694–00-0005) and the negative control/SiScramble (Non-targeting pool siRNA, D-001810–10-05) were purchased from Dharmacon. We transfected bEnd.3 cells when 70% confluent with 60nM siRNA per six-well plate. Experimentally, lipofectamine RNAimax (Invitrogen) is mixed with opti-MEM media (Gibco) and incubated at room temperature for 5 min (mix A). 60nM of Si*Cx43* premixed Opti-MEM is then added to mix A and incubated for 15 min (mix B). Mix B is then added to bEnd.3 cells DMEM media (ATCC) without penicillin/streptomycin. The same protocol was used to transfect ANS4-GFP cells with 40nM of Si*Cx43*. 60nM and 40nM of SiScramble (control) were used to transfect bEnd.3 and ANS4-GFP cells, respectively, for control experiments. Cells were used for experiments 72 h post-transfection.

***Gja1* overexpression in ANS4-GFP—**Gja1 overexpression in ANS4-GFP was performed using a pcDNA3.1^{+}/C-(K)DYK vector containing *mus musculus Gja1* (*Cx43*) cDNA (GenScript NM_010288.3). Transfection was performed in 6-well plate with Lipofectamine 2000. To assess proliferation, EdU (5μM) was added to the culture media 24 h post-transfection. At 48 h post-transfection, NSC-GFP were collected for qPCR and Western blot analysis to assess transgene expression or fixed for immunofluorescence studies to assess *Cx43* expression and EdU uptake.

Generation of Cx43 mutants—Human *GJA1* (gene for *Cx43*) full length (FL) construct, Cx43 cytoplasmic tail truncated at amino acid 258 (*Cx43ΔCT258*) and dead channel Cx43 mutant (*Cx43T154A*, mutation that converts threonine 154 into alanine) were PCR-amplified from pTRE-TIGHT-Cx43-eYFP (gifted from Robin Shaw; Addgene Plasmid #31807) and cloned into the pcDNA3.1-HA (gifted from Oskar Laur; Addgene Plasmid #128034). We inserted the PCR fragments at NheI/BamHI sites by infusion HD-cloning (Takara Biosciences), to excise HA-tag from the plasmid, rendering the constructs expressed as tag-less. Site-directed mutagenesis was achieved using Q5Site-Directed Mutagenesis Kit (NEB, USA). Primers were designed using NEB-Base changer software (Table S3). Plasmids were sequenced and confirmed by Eurofin Sanger Sequencing Services, USA.

Cell culture—ANS4-GFP cells were gifted from Dr. Steve M. Pollard (University of Edinburgh). The ANS4-GFP cells are representative of adult NSCs in the SVZ, as they express genes enriched in adult NSCs and are capable of differentiating into neurons and astrocytes when subjected to a permissive differentiation environment bEnd.3 cells were purchased from (ATCC CRL-2299) and cultured in Dulbecco's Modified Eagle's Medium (DMEM) (ATCC 30–2002) supplemented with 10% FBS and 1% penicillin/streptomycin. ANS4-GFP cells were used up to passage (P) 30 and bEnd.3 up to P16.

Transwell co-culture of bEnd.3 and ANS4-GFP—Transwell polycarbonate membranes of a 12-well plate (Corning, catalog #3401) were activated with media and bottom sides were pre-coated with 0.1% gelatin for 1 h at 37°C. The transwell inserts were then placed with bottom side facing up in a 100mm tissue culture dish pre-filled with DPBS and bEnd.3 were then seeded. One hour later, inserts were flipped back in the wells of the 12-well plate pre-filled with bEnd.3 media and top side was coated with laminin (10 μg/ml overnight at 37°C). 24 hr-post-bEnd.3 seeding, the membrane was washed on both sides with serum free media to remove any traces of serum that may cause differentiation of ANS4-GFP cells. ANS4-GFP cells were then seeded on the top side of membrane in ANS4 media without growth factors (EGF and FGF). bEnd.3 and ANS4 were co-cultured at a 1:2 ratio in 100% ANS4-GFP media (supplemented with 5μM EdU when needed). Membranes designated for ANS4-GFP monocultures were subjected to the same extracellular matrix coating proteins as co-culture studies. ANS4-GFP were harvested after 48 h of co-culture with trypsin for either qPCR analysis or fixed with 3.7% pre-warmed formaldehyde for immunofluoresence studies. For *Gja1* knock-down studies: bEnd.3 cells seeded on the bottom side of the membrane were transfected 24 h before seeding ANS4-GFP cells on the top side and subjected to 48 h of co-culture prior to harvest. For studies using si*Cx43* transfected ANS4-GFP: ANS4-GFP were transfected 24 h prior to seeding on the top side of the membrane and harvested after 48 h of co-culture. For studies using human *GJA1* mutants, ANS4-GFP and bEnd.3 were treated concomitantly with Si*Cx43* (see section siRNA transfection) and/or Cx43FL (1μg), Cx43T154A (0.5 μg), Cx43CTΔ258 (1 μg) for 6 h. After Si*Cx43* and DNA transfection, cells were subjected to a media change and harvested after 48 h of co-culture. To block Cx43 channel activity, after 24 h of co-culture, ANS4-GFP and bEnd.3 cells were both treated with 100nM of ^{43}gap 26 peptide (VCYDKSFPISHVR) (Genscript, catalog # RP20274), every 8 h for 24 h. To block ERK signaling in the co-culture system, ANS4-GFP cells were treated with 10μM of U0126 (Cell signaling catalog #9903S) for 24 h. ANS4-GFP were collected (6–8 wells are pooled per condition) either for qPCR or Western blot analysis after 48 h of co-culture.

Immunofluorescence of transwell membranes—Insert wells were washed with DPBS supplemented with Ca^{2+} and Mg^{2+} allowing for cells to remain attached to the membrane. Cells were fixed with pre-warmed 3.7% formaldehyde in DPBS supplement with Ca^{2+} and Mg^{2+} for 15 min, then permeabilized with 0.5% Triton X-100 in PBS at room temperature for 20 min prior to EdU staining (Click-iT, Invitrogen). Cells were then blocked with 10% donkey serum and 0.1% Triton X-100 (blocking buffer) for 1 h at RT followed by incubation with primary antibodies, chicken anti-GFP (1:500, Abcam ab13970) for NSCs and hamster anti-CD31 (1:500, Millipore MAB1398Z) for bEnd.3 cells, in blocking buffer at 4°C overnight and corresponding conjugated secondary antibodies for 1 h at RT. Hoechst (5 μg/mL) was used for nuclear counterstaining. Membranes were cut out from inserts and mounted with DAKO mounting media (Agilent). Images were acquired with a DMi8 SP8 confocal microscope at 4 different viewing fields and analyzed in ImageJ.

Bulk RNA sequencing—mRNA samples from ANS4-GFP and ANS4-GFP cells co-cultured with bEnd.3 (for 72 h) were isolated using RNeasy Plus Micro Kit (QIAGEN, cat# 74034). Next-generation whole transcriptome Illumina sequencing (HiSeq4000) was

performed by the Yale Center for Genome Analysis. Fastq-files of raw reads were generated with bcl2fastq2_v2.19.0 and then uploaded to the usegalaxy.org platform[75] for quality control and trimming (Galaxy ToolShed v 1.0.2; FASTQ/A short-reads pre-processing tools: http://hannonlab.cshl.edu/fastx_toolkit/).[76,77] Sequences were aligned to the hg38genome using Kallisto[78] and aligned sequences were quantified with Sleuth.[79] Differential gene expression analysis was performed with the Sleuth package in R by the Likelihood Ratio Test with regression of the experiment number to account for batch effects.

Western Blot—Cells were lysed in RIPA buffer (Abcam, ab206996) and equal amounts of proteins (quantified with Pierce BCA assay kit, Thermo Fisher, 23252) were separated on 4–15% gradient Criterion precast gels (Bio-Rad 567–1084). Proteins were then transferred onto nitrocellulose membranes (Bio-Rad). Western Blots were developed with chemiluminescence HRP substrate (Radiance plus, Azure Biosystems AC2103) on a digital image analyzer, Azure Imager c300. Uncropped western blots are shown in Figure S9.

Label retaining cell (LRC) protocol—Wild-type mice received BrdU (7.5 mg/ml) i.p injections twice daily for 5 days and sacrificed 4 wk after the last injection. Quantification of connexin protein colocalization with LRCs or ECs was performed on confocal z stack images by a computational approach using FARSIGHT for nuclear segmentation and MATLAB.[34]

QUANTIFICATION AND STATISTICAL ANALYSIS

Data analysis and statistics—The Mann-Whitney non-parametric test for unpaired samples was used to analyze continuous variables between groups. When two or more groups were being compared, the parametric two-way ANOVA statistical test with Sidak's multiple comparison was performed. All continuous variables are represented as mean ± SEM. p value ≤0.05 was considered statistically significant. All analyses were performed using Prism 8.0 software (GraphPad). All statistical details of experiments can be found in the figure legends.

Supplementary Material

Refer to Web version on PubMed Central for supplementary material.

ACKNOWLEDGMENTS

The authors of this work were supported by NIH grants to K.K.H. (R01 EB 016629, HL146056, and NIH U2EB017103), an AHA postdoctoral fellowship to N.G. (19POST34400065), an AHA Career Development Award to G.G. (938744), NIH grants to N.W.C. (T32 HL007224 and T32 HL007284), and a Wellcome Trust Senior Investigator Award to C.ff.-C.

REFERENCES

1. Chaker Z, Codega P, and Doetsch F. (2016). A mosaic world: puzzles revealed by adult neural stem cell heterogeneity. Wiley Interdiscip. Rev. Dev. Biol 5, 640–658. 10.1002/wdev.248. [PubMed: 27647730]

2. Doetsch F, Garcá-Verdugo JM, and Alvarez-Buylla A. (1997). Cellular composition and three-dimensional organization of the subventricular germinal zone in the adult mammalian brain. J. Neurosci 17, 5046–5061. [PubMed: 9185542]

3. Parras CM, Schuurmans C, Scardigli R, Kim J, Anderson DJ, and Guillemot F. (2002). Divergent functions of the proneural genes Mash1 and Ngn2 in the specification of neuronal subtype identity. Genes Dev. 16, 324–338. 10.1101/gad.940902. [PubMed: 11825874]
4. Pastrana E, Cheng LC, and Doetsch F. (2009). Simultaneous prospective purification of adult subventricular zone neural stem cells and their progeny. Proc. Natl. Acad. Sci. USA 106, 6387–6392. 10.1073/pnas.0810407106. [PubMed: 19332781]
5. Doetsch F, Caillé I, Lim DA, García-Verdugo JM, and Alvarez-Buylla A. (1999). Subventricular zone astrocytes are neural stem cells in the adult mammalian brain. Cell 97, 703–716. 10.1016/s0092-8674(00)80783-7. [PubMed: 10380923]
6. Doetsch F, García-Verdugo JM, and Alvarez-Buylla A. (1999). Regeneration of a germinal layer in the adult mammalian brain. Proc. Natl. Acad. Sci. USA 96, 11619–11624. 10.1073/pnas.96.20.11619. [PubMed: 10500226]
7. Mirzadeh Z, Merkle FT, Soriano-Navarro M, Garcia-Verdugo JM, and Alvarez-Buylla A. (2008). Neural stem cells confer unique pinwheel architecture to the ventricular surface in neurogenic regions of the adult brain. Cell Stem Cell 3, 265–278. 10.1016/j.stem.2008.07.004. [PubMed: 18786414]
8. Gleeson JG, Lin PT, Flanagan LA, and Walsh CA (1999). Doublecortin is a microtubule-associated protein and is expressed widely by migrating neurons. Neuron 23, 257–271. 10.1016/s0896-6273(00)80778-3. [PubMed: 10399933]
9. Lois C, and Alvarez-Buylla A. (1994). Long-distance neuronal migration in the adult mammalian brain. Science 264, 1145–1148. 10.1126/science.8178174. [PubMed: 8178174]
10. Menezes JR, Smith CM, Nelson KC, and Luskin MB (1995). The division of neuronal progenitor cells during migration in the neonatal mammalian forebrain. Mol. Cell. Neurosci 6, 496–508. 10.1006/mcne.1995.0002. [PubMed: 8742267]
11. Altman J. (1969). Autoradiographic and histological studies of postnatal neurogenesis. IV. Cell proliferation and migration in the anterior forebrain, with special reference to persisting neurogenesis in the olfactory bulb. J. Comp. Neurol 137, 433–457. 10.1002/cne.901370404. [PubMed: 5361244]
12. Luskin MB (1993). Restricted proliferation and migration of postnatally generated neurons derived from the forebrain subventricular zone. Neuron 11, 173–189. 10.1016/0896-6273(93)90281-u. [PubMed: 8338665]
13. Corotto FS, Henegar JA, and Maruniak JA (1993). Neurogenesis persists in the subependymal layer of the adult mouse brain. Neurosci. Lett 149, 111–114. 10.1016/0304-3940(93)90748-a. [PubMed: 8474679]
14. James R, Kim Y, Hockberger PE, and Szele FG (2011). Subventricular zone cell migration: lessons from quantitative two-photon microscopy. Front. Neurosci 5, 30. 10.3389/fnins.2011.00030. [PubMed: 21472025]
15. Obernier K, Cebrian-Silla A, Thomson M, Parraguez JI, Anderson R,Guinto C, Rodas Rodriguez J, Garcia-Verdugo JM, and Alvarez-Buylla A. (2018). Adult neurogenesis is sustained by symmetric self-renewal and differentiation. Cell Stem Cell 22, 221–234.e8. 10.1016/j.stem.2018.01.003. [PubMed: 29395056]
16. Silva-Vargas V, Delgado AC, and Doetsch F. (2018). Symmetric stem cell division at the Heart of adult neurogenesis. Neuron 98, 246–248. 10.1016/j.neuron.2018.04.005. [PubMed: 29673477]
17. Shen Q, Wang Y, Kokovay E, Lin G, Chuang SM, Goderie SK, Roysam B, and Temple S. (2008). Adult SVZ stem cells lie in a vascular niche: a quantitative analysis of niche cell-cell interactions. Cell Stem Cell 3, 289–300. 10.1016/j.stem.2008.07.026. [PubMed: 18786416]
18. Tavazoie M, Van der Veken L, Silva-Vargas V, Louissaint M, Colonna L, Zaidi B, Garcia-Verdugo JM, and Doetsch F. (2008). A specialized vascular niche for adult neural stem cells. Cell Stem Cell 3, 279–288. 10.1016/j.stem.2008.07.025. [PubMed: 18786415]
19. Calvo CF, Fontaine RH, Soueid J, Tammela T, Makinen T, Alfaro-Cervello C, Bonnaud F, Miguez A, Benhaim L, Xu Y, et al. (2011). Vascular endothelial growth factor receptor 3 directly regulates murine neurogenesis. Genes Dev. 25, 831–844. 10.1101/gad.615311. [PubMed: 21498572]

20. Jin K, Zhu Y, Sun Y, Mao XO, Xie L, and Greenberg DA (2002). Vascular endothelial growth factor (VEGF) stimulates neurogenesis in vitro and in vivo. Proc. Natl. Acad. Sci. USA 99, 11946–11950. 10.1073/pnas.182296499. [PubMed: 12181492]
21. Gómez-Gaviro MV, Scott CE, Sesay AK, Matheu A, Booth S, Galichet C, and Lovell-Badge R. (2012). Betacellulin promotes cell proliferation in the neural stem cell niche and stimulates neurogenesis. Proc. Natl. Acad. Sci. USA 109, 1317–1322. 10.1073/pnas.1016199109. [PubMed: 22232668]
22. Ramírez-Castillejo C, Sánchez-Sánchez F, Andreu-Agulló C, Ferrón SR, Aroca-Aguilar JD, Sánchez P, Mira H, Escribano J, and Fariñas I. (2006). Pigment epithelium-derived factor is a niche signal for neural stem cell renewal. Nat. Neurosci 9, 331–339. 10.1038/nn1657. [PubMed: 16491078]
23. Crouch EE, Liu C, Silva-Vargas V, and Doetsch F. (2015). Regional and stage-specific effects of prospectively purified vascular cells on the adult V-SVZ neural stem cell lineage. J. Neurosci 35, 4528–4539. 10.1523/JNEUROSCI.1188-14.2015. [PubMed: 25788671]
24. Genet N, and Hirschi KK (2021). Understanding neural stem cell regulation in vivo and applying the insights to cell therapy for strokes. Regen. Med 16, 861–870. 10.2217/rme-2021-0022_(2021. [PubMed: 34498495]
25. Ottone C, Krusche B, Whitby A, Clements M, Quadrato G, Pitulescu ME, Adams RH, and Parrinello S. (2014). Direct cell-cell contact with the vascular niche maintains quiescent neural stem cells. Nat. Cell Biol 16, 1045–1056. 10.1038/ncb3045. [PubMed: 25283993]
26. Bicker F, Vasic V, Horta G, Ortega F, Nolte H, Kavyanifar A, Keller S, Stankovic ND, Harter PN, Benedito R, et al. (2017). Neurovascular EGFL7 regulates adult neurogenesis in the subventricular zone and thereby affects olfactory perception. Nat. Commun 8, 15922. 10.1038/ncomms15922. [PubMed: 28656980]
27. Miragall F, Albiez P, Bartels H, de Vries U, and Dermietzel R. (1997). Expression of the gap junction protein connexin43 in the subependymal layer and the rostral migratory stream of the mouse: evidence for an inverse correlation between intensity of connexin43 expression and cell proliferation activity. Cell Tissue Res. 287, 243–253. 10.1007/s004410050749. [PubMed: 8995195]
28. Nadarajah B, Jones AM, Evans WH, and Parnavelas JG (1997). Differential expression of connexins during neocortical development and neuronal circuit formation. J. Neurosci 17, 3096–3111. [PubMed: 9096144]
29. Bittman KS, and LoTurco JJ (1999). Differential regulation of connexin 26 and 43 in murine neocortical precursors. Cereb. Cortex 9, 188–195. 10.1093/cercor/9.2.188. [PubMed: 10220231]
30. Pollard SM, Conti L, Sun Y, Goffredo D, and Smith A. (2006). Adherent neural stem (NS) cells from fetal and adult forebrain. Cereb. Cortex 16 (Suppl 1), i112–i120. 10.1093/cercor/bhj167. [PubMed: 16766697]
31. Hirschi KK, Burt JM, Hirschi KD, and Dai C. (2003). Gap junction communication mediates transforming growth factor-beta activation and endothelial-induced mural cell differentiation. Circ. Res 93, 429–437. 10.1161/01.RES.0000091259.84556.D5. [PubMed: 12919949]
32. Swayne LA, and Bennett SAL (2016). Connexins and pannexins in neuronal development and adult neurogenesis. BMC Cell Biol. 17 (Suppl 1), 10. 10.1186/s12860-016-0089-5. [PubMed: 27230672]
33. Zhao Y, Xin Y, He Z, and Hu W. (2018). Function of connexins in the interaction between glial and vascular cells in the central nervous system and related neurological diseases. Neural Plast. 2018, 6323901. 10.1155/2018/6323901.
34. Goldberg JS, Vadakkan TJ, Hirschi KK, and Dickinson ME (2013). A computational approach to detect gap junction plaques and associate them with cells in fluorescent images. J. Histochem. Cytochem 61, 283–293. 10.1369/0022155413477114. [PubMed: 23324867]
35. Brazel CY, Limke TL, Osborne JK, Miura T, Cai J, Pevny L, and Rao MS (2005). Sox2 expression defines a heterogeneous population of neurosphere-forming cells in the adult murine brain. Aging Cell 4, 197–207. 10.1111/j.1474-9726.2005.00158.x. [PubMed: 16026334]

36. Mercurio S, Serra L, and Nicolis SK (2019). More than just stem cells: functional roles of the transcription factor Sox2 in differentiated glia and neurons. Int. J. Mol. Sci 20, 4540. 10.3390/ijms20184540. [PubMed: 31540269]
37. Boulay AC, Mazeraud A, Cisternino S, Saubaméa B, Mailly P, Jourdren L, Blugeon C, Mignon V, Smirnova M, Cavallo A, et al. (2015). Immune quiescence of the brain is set by astroglial connexin 43. J. Neurosci 35, 4427–4439. 10.1523/JNEUROSCI.2575-14.2015. [PubMed: 25762685]
38. Chew SSL, Johnson CS, Green CR, and Danesh-Meyer HV (2010). Role of connexin43 in central nervous system injury. Exp. Neurol 225, 250–261. 10.1016/j.expneurol.2010.07.014. [PubMed: 20655909]
39. Danesh-Meyer HV, and Green CR (2008). Focus on molecules: connexin 43–mind the gap. Exp. Eye Res 87, 494–495. 10.1016/j.exer.2008.01.021. [PubMed: 18342308]
40. Dulken BW, Leeman DS, Boutet SC, Hebestreit K, and Brunet A. (2017). Single-cell transcriptomic analysis defines heterogeneity and transcriptional dynamics in the adult neural stem cell lineage. Cell Rep. 18, 777–790. 10.1016/j.celrep.2016.12.060. [PubMed: 28099854]
41. Chavkin NW, Genet G, Poulet M, Jeffery ED, Marziano C, Genet N, Vasavada H, Nelson EA, Acharya BR, Kour A, et al. (2022). Endothelial cell cycle state determines propensity for arterial-venous fate. Nat. Commun 13, 5891. 10.1038/s41467-022-33324-7_(2022. [PubMed: 36202789]
42. Llorens-Bobadilla E, Zhao S, Baser A, Saiz-Castro G, Zwadlo K, and Martin-Villalba A. (2015). Single-cell transcriptomics reveals a population of Dormant neural stem cells that become activated upon brain injury. Cell Stem Cell 17, 329–340. 10.1016/j.stem.2015.07.002. [PubMed: 26235341]
43. Cebrian-Silla A, Nascimento MA, Redmond SA, Mansky B, Wu D, Obernier K, Romero Rodriguez R, Gonzalez-Granero S, García-Verdugo JM, Lim DA, and Álvarez-Buylla A. (2021). Single-cell analysis of the ventricular-subventricular zone reveals signatures of dorsal and ventral adult neurogenesis. Elife 10, e67436. 10.7554/eLife.67436.
44. Kokovay E, Wang Y, Kusek G, Wurster R, Lederman P, Lowry N, Shen Q, and Temple S. (2012). VCAM1 is essential to maintain the structure of the SVZ niche and acts as an environmental sensor to regulate SVZ lineage progression. Cell Stem Cell 11, 220–230. 10.1016/j.stem.2012.06.016. [PubMed: 22862947]
45. DeVos SL, and Miller TM (2013). Direct intraventricular delivery of drugs to the rodent central nervous system. J. Vis. Exp, e50326. 10.3791/50326.
46. Beahm DL, Oshima A, Gaietta GM, Hand GM, Smock AE, Zucker SN, Toloue MM, Chandrasekhar A, Nicholson BJ, and Sosinsky GE (2006). Mutation of a conserved threonine in the third transmembrane helix of alpha- and beta-connexins creates a dominant-negative closed gap junction channel. J. Biol. Chem 281, 7994–8009. 10.1074/jbc.M506533200. [PubMed: 16407179]
47. Maass K, Shibayama J, Chase SE, Willecke K, and Delmar M(2007). C-terminal truncation of connexin43 changes number, size, and localization of cardiac gap junction plaques. Circ. Res 101, 1283–1291. 10.1161/CIRCRESAHA.107.162818. [PubMed: 17932323]
48. Genet N, Bhatt N, Bourdieu A, and Hirschi KK (2018). Multifacetedroles of connexin 43 in stem cell niches. Curr. Stem Cell Rep. 4, 1–12. 10.1007/s40778-018-0110-3.
49. Moorer MC, Hebert C, Tomlinson RE, Iyer SR, Chason M, andStains JP (2017). Defective signaling, osteoblastogenesis and bone remodeling in a mouse model of connexin 43 C-terminal truncation. J. Cell Sci 130, 531–540. 10.1242/jcs.197285. [PubMed: 28049723]
50. Liu F, Yang X, Geng M, and Huang M. (2018). Targeting ERK, an Achilles' Heel of the MAPK pathway, in cancer therapy. Acta Pharm. Sin. B 8, 552–562. 10.1016/j.apsb.2018.01.008. [PubMed: 30109180]
51. Zheng L, Li H, Cannon A, Trease AJ, Spagnol G, Zheng H, Radio S, Patel K, Batra S, and Sorgen PL (2019). Phosphorylation of Cx43 residue Y313 by Src contributes to blocking the interaction with Drebrin and disassembling gap junctions. J. Mol. Cell. Cardiol 126, 36–49. 10.1016/j.yjmcc.2018.11.008. [PubMed: 30448479]
52. Andreu-Agulló C, Morante-Redolat JM, Delgado AC, and Fariñas I. (2009). Vascular niche factor PEDF modulates Notch-dependent stemness in the adult subependymal zone. Nat. Neurosci 12, 1514–1523. 10.1038/nn.2437. [PubMed: 19898467]

53. Kirschenbaum B, and Goldman SA (1995). Brain-derived neurotrophic factor promotes the survival of neurons arising from the adult rat forebrain subependymal zone. Proc. Natl. Acad. Sci. USA 92, 210–214. 10.1073/pnas.92.1.210. [PubMed: 7816819]
54. Kokovay E, Goderie S, Wang Y, Lotz S, Lin G, Sun Y, Roysam B, Shen Q, and Temple S. (2010). Adult SVZ lineage cells home to and leave the vascular niche via differential responses to SDF1/CXCR4 signaling. Cell Stem Cell 7, 163–173. 10.1016/j.stem.2010.05.019. [PubMed: 20682445]
55. Leventhal C, Rafii S, Rafii D, Shahar A, and Goldman SA (1999). Endothelial trophic support of neuronal production and recruitment from the adult mammalian subependyma. Mol. Cell. Neurosci 13, 450–464. 10.1006/mcne.1999.0762. [PubMed: 10383830]
56. Snapyan M, Lemasson M, Brill MS, Blais M, Massouh M, Ninkovic J, Gravel C, Berthod F, Götz M, Barker PA, et al. (2009). Vasculature guides migrating neuronal precursors in the adult mammalian forebrain via brain-derived neurotrophic factor signaling. J. Neurosci 29, 4172–4188. 10.1523/JNEUROSCI.4956-08.2009. [PubMed: 19339612]
57. Cheng A, Tang H, Cai J, Zhu M, Zhang X, Rao M, and Mattson MP (2004). Gap junctional communication is required to maintain mouse cortical neural progenitor cells in a proliferative state. Dev. Biol 272, 203–216. 10.1016/j.ydbio.2004.04.031. [PubMed: 15242801]
58. Duval N, Gomès D, Calaora V, Calabrese A, Meda P, and Bruzzone R. (2002). Cell coupling and *Cx43* expression in embryonic mouse neural progenitor cells. J. Cell Sci 115, 3241–3251. [PubMed: 12140256]
59. Ravella A, Ringstedt T, Brion JP, Pandolfo M, and Herlenius E(2015). Adult neural precursor cells form connexin-dependent networks that improve their survival. Neuroreport 26, 928–936. 10.1097/WNR.0000000000000451. [PubMed: 26351758]
60. Todorova MG, Soria B, and Quesada I. (2008). Gap junctional intercellular communication is required to maintain embryonic stem cells in a non-differentiated and proliferative state. J. Cell. Physiol 214, 354–362. 10.1002/jcp.21203. [PubMed: 17654515]
61. Shi Z, Geng Y, Liu J, Zhang H, Zhou L, Lin Q, Yu J, Zhang K, Liu J, Gao X, et al. (2018). Single-cell transcriptomics reveals gene signatures and alterations associated with aging in distinct neural stem/progenitor cell subpopulations. Protein Cell 9, 351–364. 10.1007/s13238-017-0450-2. [PubMed: 28748452]
62. Qi GJ, Chen Q, Chen LJ, Shu Y, Bu LL, Shao XY, Zhang P, Jiao FJ, Shi J, and Tian B. (2016). Phosphorylation of connexin 43 by Cdk5 modulates neuronal migration during embryonic brain development. Mol. Neurobiol 53, 2969–2982. 10.1007/s12035-015-9190-6. [PubMed: 25952543]
63. Jeon SH, Yoon JY, Park YN, Jeong WJ, Kim S, Jho EH, Surh YJ, and Choi KY (2007). Axin inhibits extracellular signal-regulated kinase pathway by Ras degradation via beta-catenin. J. Biol. Chem 282, 14482–14492. 10.1074/jbc.M611129200. [PubMed: 17374607]
64. Xu J, Lim SBH, Ng MY, Ali SM, Kausalya JP, Limviphuvadh V, Maurer-Stroh S, and Hunziker W. (2012). ZO-1 regulates Erk, Smad1/5/8, Smad2, and RhoA activities to modulate self-renewal and differentiation of mouse embryonic stem cells. Stem Cell. 30, 1885–1900. 10.1002/stem.1172.
65. Zhang J, Griemsmann S, Wu Z, Dobrowolski R, Willecke K, Theis M,Steinhäuser C, and Bedner P. (2018). Connexin43, but not connexin30, contributes to adult neurogenesis in the dentate gyrus. Brain Res. Bull 136, 91–100. 10.1016/j.brainresbull.2017.07.001. [PubMed: 28689039]
66. Codega P, Silva-Vargas V, Paul A, Maldonado-Soto AR, Deleo AM, Pastrana E, and Doetsch F. (2014). Prospective identification and purification of quiescent adult neural stem cells from their *in vivo* niche. Neuron 82, 545–559. 10.1016/j.neuron.2014.02.039. [PubMed: 24811379]
67. Sörensen I, Adams RH, and Gossler A. (2009). DLL1-mediated Notch activation regulates endothelial identity in mouse fetal arteries. Blood 113, 5680–5688. 10.1182/blood-2008-08-174508. [PubMed: 19144989]
68. Wang Y, Nakayama M, Pitulescu ME, Schmidt TS, Bochenek ML, Sakakibara A, Adams S, Davy A, Deutsch U, Lüthi U, et al. (2010). Ephrin-B2 controls VEGF-induced angiogenesis and lymphangiogenesis. Nature 465, 483–486. 10.1038/nature09002. [PubMed: 20445537]
69. Mori T, Tanaka K, Buffo A, Wurst W, Kühn R, and Götz M. (2006). Inducible gene deletion in astroglia and radial glia–a valuable tool for functional and lineage analysis. Glia 54, 21–34. 10.1002/glia.20350. [PubMed: 16652340]

70. Cotsarelis G, Cheng SZ, Dong G, Sun TT, and Lavker RM (1989). Existence of slow-cycling limbal epithelial basal cells that can be preferentially stimulated to proliferate: implications on epithelial stem cells. Cell 57, 201–209. 10.1016/0092-8674(89)90958-6. [PubMed: 2702690]
71. Potten CS, and Morris RJ (1988). Epithelial stem cells *in vivo*. J. Cell Sci Suppl. 10, 45–62. 10.1242/jcs.1988.supplement_10.4.
72. Crouch EE, and Doetsch F. (2018). FACS isolation of endothelial cells and pericytes from mouse brain microregions. Nat. Protoc 13, 738–751. 10.1038/nprot.2017.158. [PubMed: 29565899]
73. Kazanis I, Lathia JD, Vadakkan TJ, Raborn E, Wan R, Mughal MR, Eckley DM, Sasaki T, Patton B, Mattson MP, et al. (2010). Quiescence and activation of stem and precursor cell populations in the subependymal zone of the mammalian brain are associated with distinct cellular and extracellular matrix signals. J. Neurosci 30, 9771–9781. 10.1523/JNEUROSCI.0700-10.2010. [PubMed: 20660259]
74. Livak KJ, and Schmittgen TD (2001). Analysis of relative gene expression data using real-time quantitative PCR and the 2(-Delta Delta C(T)) Method. Methods 25, 402–408. 10.1006/meth.2001.1262. [PubMed: 11846609]
75. Afgan E, Baker D, Batut B, van den Beek M, Bouvier D, Cech M, Chilton J, Clements D, Coraor N, Grüning BA, et al. (2018). The Galaxy platform for accessible, reproducible and collaborative biomedical analyses: 2018 update. Nucleic Acids Res. 46, W537–W544. 10.1093/nar/gky379. [PubMed: 29790989]
76. Blankenberg D, Gordon A, Von Kuster G, Coraor N, Taylor J, and Nekrutenko A; Galaxy Team (2010). Manipulation of FASTQ data with Galaxy. Bioinformatics 26, 1783–1785. 10.1093/bioinformatics/btq281. [PubMed: 20562416]
77. Blankenberg D, Von Kuster G, Coraor N, Ananda G, Lazarus R,Mangan M, Nekrutenko A, and Taylor J. (2010). Galaxy: a web-based genome analysis tool for experimentalists. Curr. Protoc. Mol. Biol Chapter 19, Unit 19.10.1–21. 10.1002/0471142727.mb1910s89.
78. Bray NL, Pimentel H, Melsted P, and Pachter L. (2016). Near-optimalprobabilistic RNA-seq quantification. Nat. Biotechnol 34, 525–527. 10.1038/nbt.3519. [PubMed: 27043002]
79. Pimentel H, Bray NL, Puente S, Melsted P, and Pachter L. (2017). Differential analysis of RNA-seq incorporating quantification uncertainty. Nat. Methods 14, 687–690. 10.1038/nmeth.4324. [PubMed: 28581496]

Highlights

- NSCs and ECs express Cx43 in the adult SVZ NSC niche
- Vascular EC-expressed Cx43 regulates adult NSC proliferation and differentiation
- Cx43 cytoplasmic tail and ERK signaling mediate Cx43 regulation of adult NSC

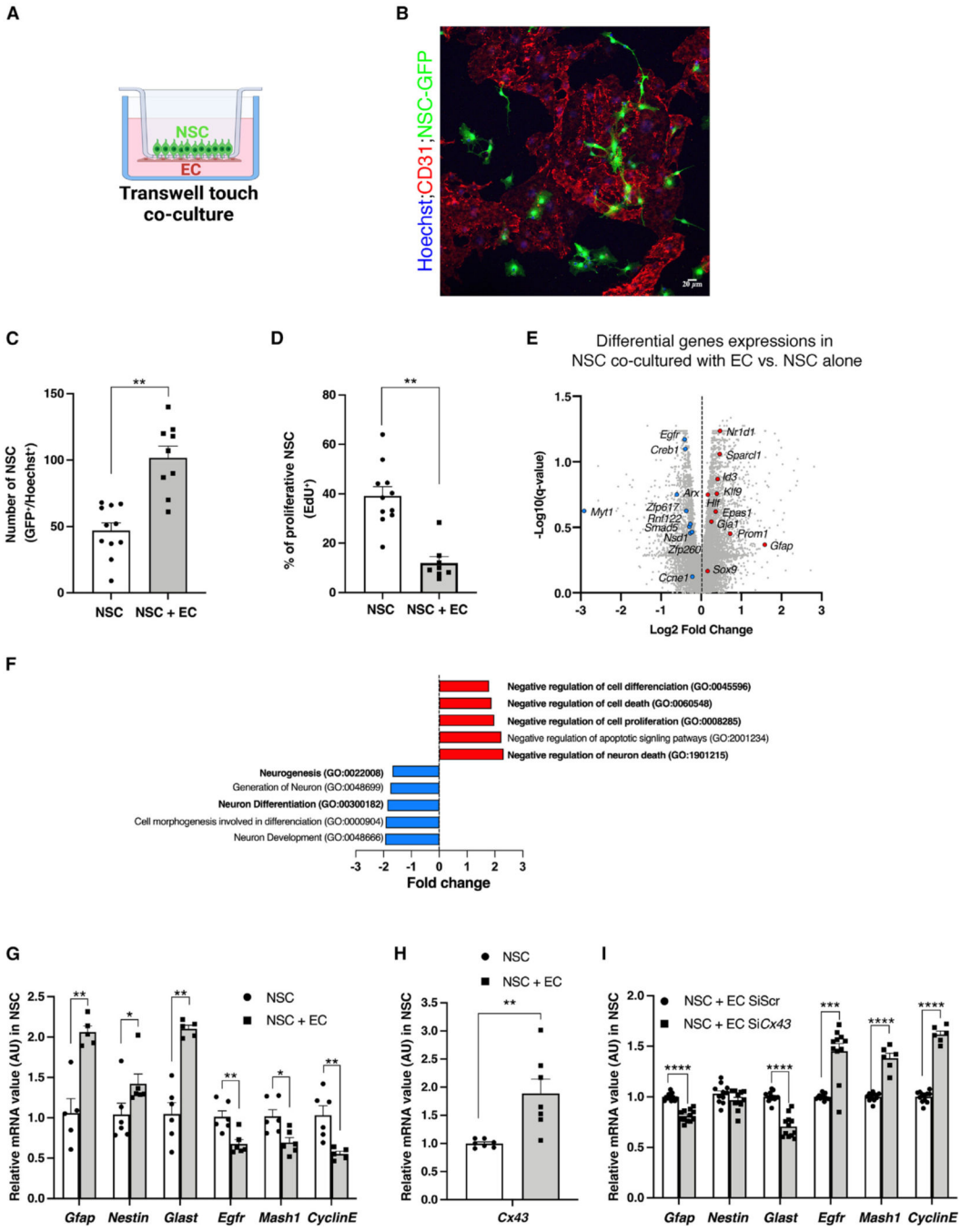

Figure 1. NSC-EC co-culture decreases NSC proliferation in a Cx43-dependent manner

(A) Schematic representation for Transwell touch co-culture of vascular ECs (bottom side) with GFP$^+$NSCs (top side). This schematic was created using BioRender.com.

(B) Confocal image showing CD31$^+$EC (red) and GFP$^+$NSCs (green) co-cultured on the Transwell membrane.

(C and D) (C) Quantification of total GFP$^+$NSCs number and (D) percentage of GFP$^+$NSCs with EdU uptake when cultured alone or with ECs respectively (n = 3 or 4 biological replicates, 4 viewing fields/n).

(E) Volcano plot of differential genes expressions in NSCs co-cultured with ECs compared with NSCs cultured alone. Red and blue dots indicate selected upregulated or downregulated genes respectively (n = 3 biological replicates).
(F) Gene Ontology term analysis of selected gene family modified in NSCs co-cultured with ECs compared with NSCs cultured alone.
(G) qPCR analysis of qNSC and aNSC genes in NSCs alone or NSCs co-cultured with ECs (n = 3 biological replicates).
(H) qPCR analysis of *Cx43* gene expression in NSCs alone or NSCs co-cultured with ECs (n = 3 biological replicates).
(I) qPCR analysis of qNSC and aNSC genes in NSCs co-cultured with ECs, where ECs are treated with control siRNA (siScr) or *Cx43* siRNA (Si*Cx43*) (n = 3 biological replicates).
Data are mean ± SEM. *p ≤ 0.05, **p ≤ 0.01, ***p ≤ 0.001, and ****p ≤ 0.0001; analysis performed using the non-parametric Mann-Whitney statistical test. See also Figures S1 and S9.

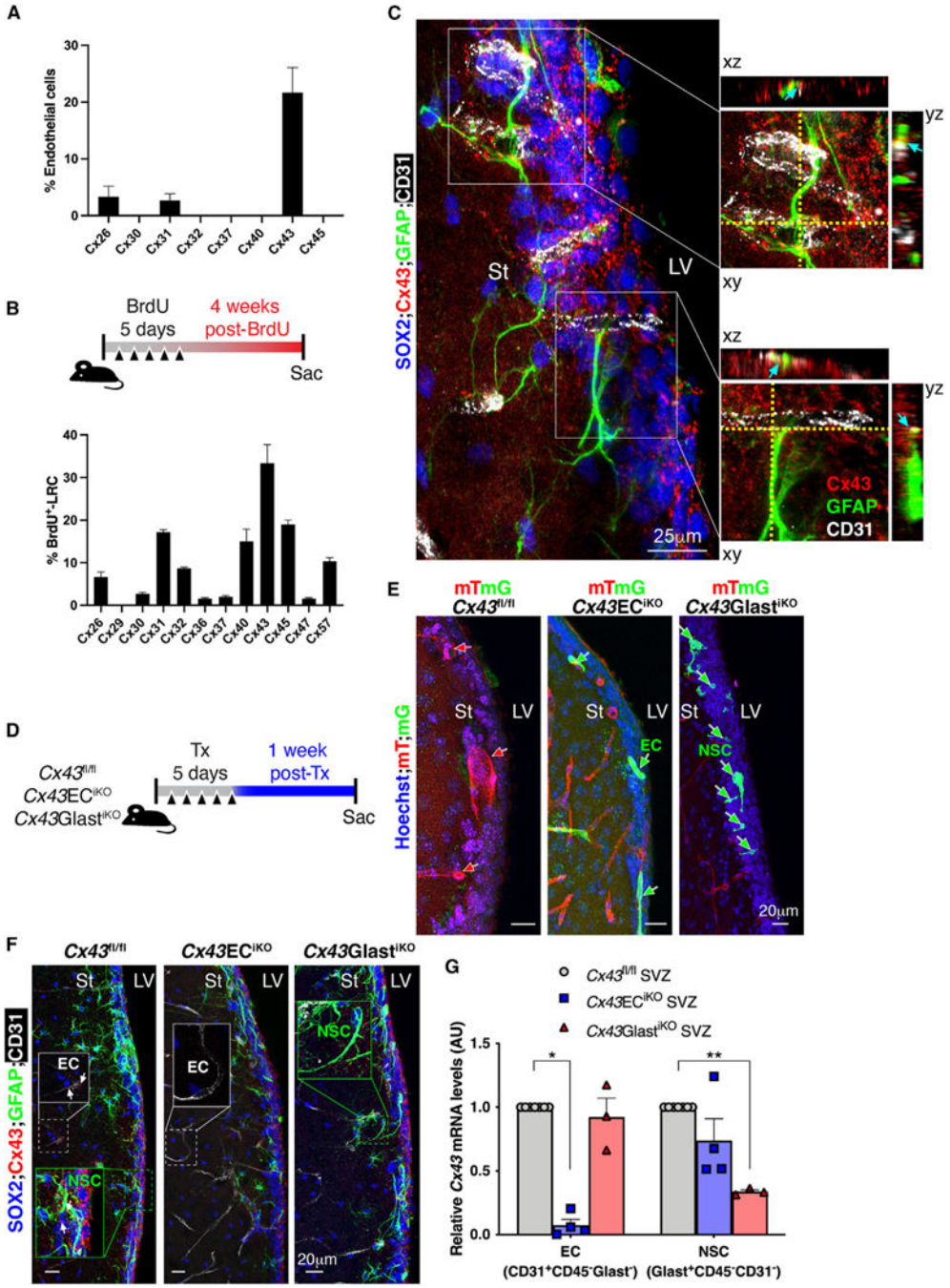

Figure 2. ECs and NSCs in the adult brain SVZ highly express Cx43

(A and B) Quantifications of the percentage of $CD31^+$-EC and $BrdU^+$-LRC^+ qNSCs colocalizing with different Cx proteins, respectively.

(C) High-resolution confocal image of a coronal SVZ section from a control mouse brain showing the endfeet of $GFAP^+SOX2^+$ NSCs (green and blue) contacting $CD31^+$ ECs (white) via Cx43 (red) punctate (insets). Orthogonal views of insets show that Cx43, ECs, and NSCs lie in close proximity marked by cyan arrows in xz and yz orientations. Scale bar, 25 μm.

(D) Timeline used to evaluate *Cx43* deletion and recombination in the SVZ.

(E) Representative confocal images of SVZ sections from *Cx43*EC^{iKO};ROSA$^{mT/mG}$ and *Cx43*Glast^{iKO};ROSA$^{mT/mG}$ mice. Note the presence of green recombinant ECs or NSCs (green arrows) and only red tomato cells in the *Cx43*$^{fl/fl}$;ROSA$^{mT/mG}$ SVZ (red arrows).
(F) Representative confocal images of Cx43 immunostaining in the SVZ sections of *Cx43*$^{fl/fl}$, *Cx43*EC^{iKO}, and *Cx43*Glast^{iKO} mice. Note that Cx43 punctate staining (white arrows) in ECs (white inset) and NSC (green inset) are specifically deleted in *Cx43*EC^{iKO} and Cx43Glast^{iKO} SVZ respectively.
(G) *Cx43* mRNA expression in ECs (CD31^{+}CD45^{-}Glast^{-} population) and NSCs (Glast^{+}CD45^{-}CD31^{-} population) of Cx43$^{fl/fl}$, *Cx43*EC^{iKO}, and *Cx43*Glast^{iKO} SVZ (n = 3–7 different experiments, 5 different mice per pooled per experiment). Scale bar, 20 μm. St, striatum; LV, lateral ventricle.
Data are mean ± SEM. *p ≤ 0.05 and **p ≤ 0.01; analysis performed using the non-parametric Mann-Whitney statistical test. See also Figures S4 and S5.

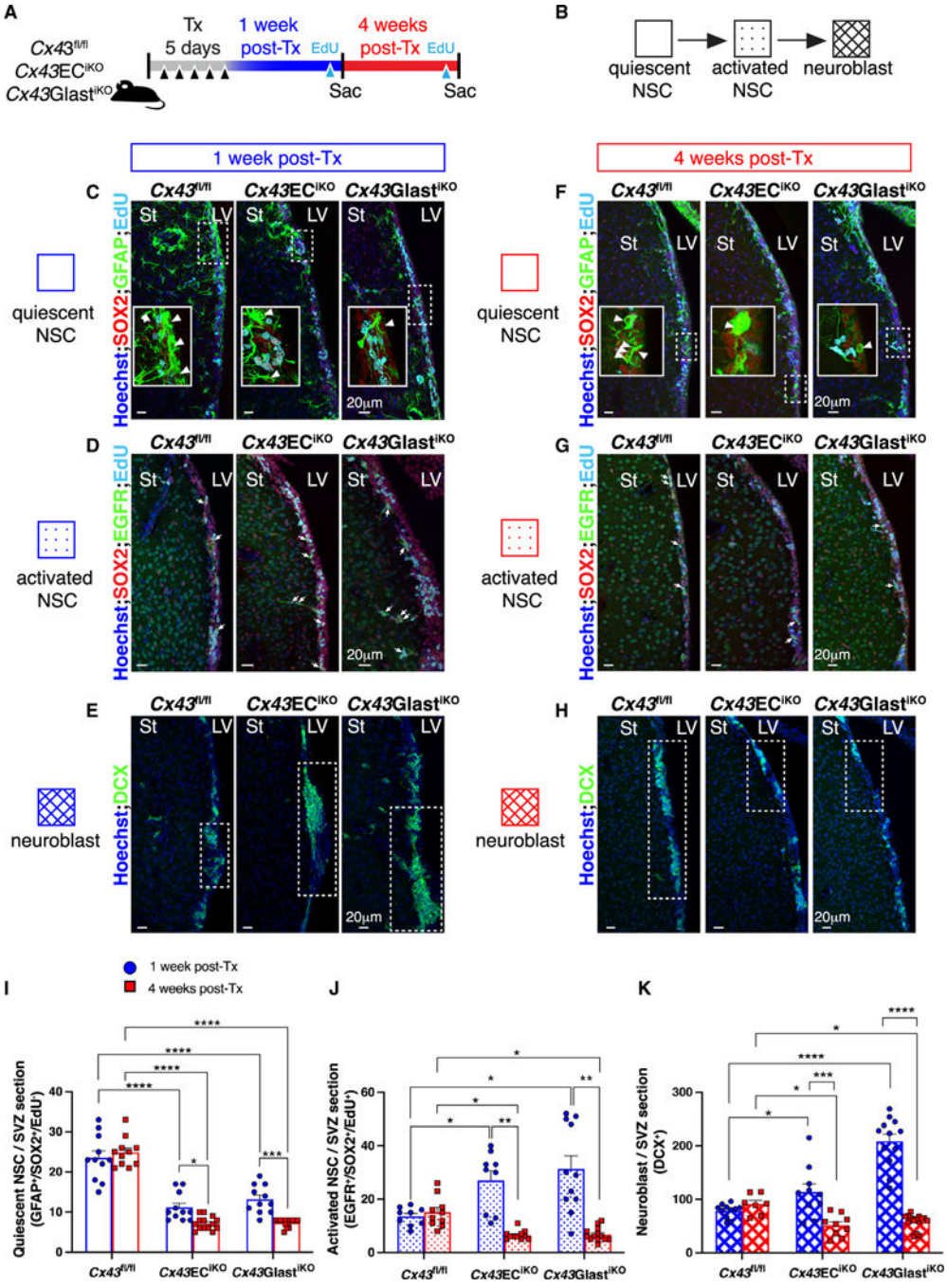

Figure 3. Cx43 deletion in ECs or NSCs depletes qNSCs in the adult SVZ

(A) Timeline used to evaluate the effects of short-term deletion (1 week post-Tx) vs. long-term deletion (4 weeks post-Tx) of *Cx43* on the number of qNSCs, aNSCs, and neuroblasts in the SVZ.

(B) Schematic model of qNSCs activation and differentiation in the SVZ.

(C–H) Confocal images of SVZ coronal sections from *Cx43*$^{fl/fl}$, *Cx43*EC^{iKO}, and *Cx43*Glast^{iKO} mice showing in (C) and (F) qNSCs (GFAP^{+}SOX2^{+}EdU^{-}, arrowheads), (D)

and (G) aNSCs ($EGFR^+SOX2^+EdU^+$, arrows), and (E) and (H) neuroblasts (DCX^+, dashed boxes) at 1 week post-Tx vs. 4 weeks post-Tx, respectively.

(I–K) Quantifications of images shown in (C)–(H). n represents the total number of different SVZ sections analyzed (technical replicates) from 3 or 4 mice per genotype. Y axes of bar graphs represent (I) number of qNSCs ($GFAP^+SOX2^+EdU^-$) per SVZ section, (J) number of aNSCs ($EGFR^+SOX2^+EdU^+$) per SVZ section, and (K) number of neuroblast (DCX^+) per SVZ section. Scale bar, 20 μm. St, striatum; LV, lateral ventricle.

Two-way ANOVA with Šidák's multiple-comparison statistical tests was used for statistical analysis, and $p \leq 0.05$ was considered to indicate statistical significance. Data are mean ± SEM. *$p \leq 0.05$, **$p \leq 0.01$, ***$p \leq 0.001$, and ****$p \leq 0.0001$. See also Figure S3.

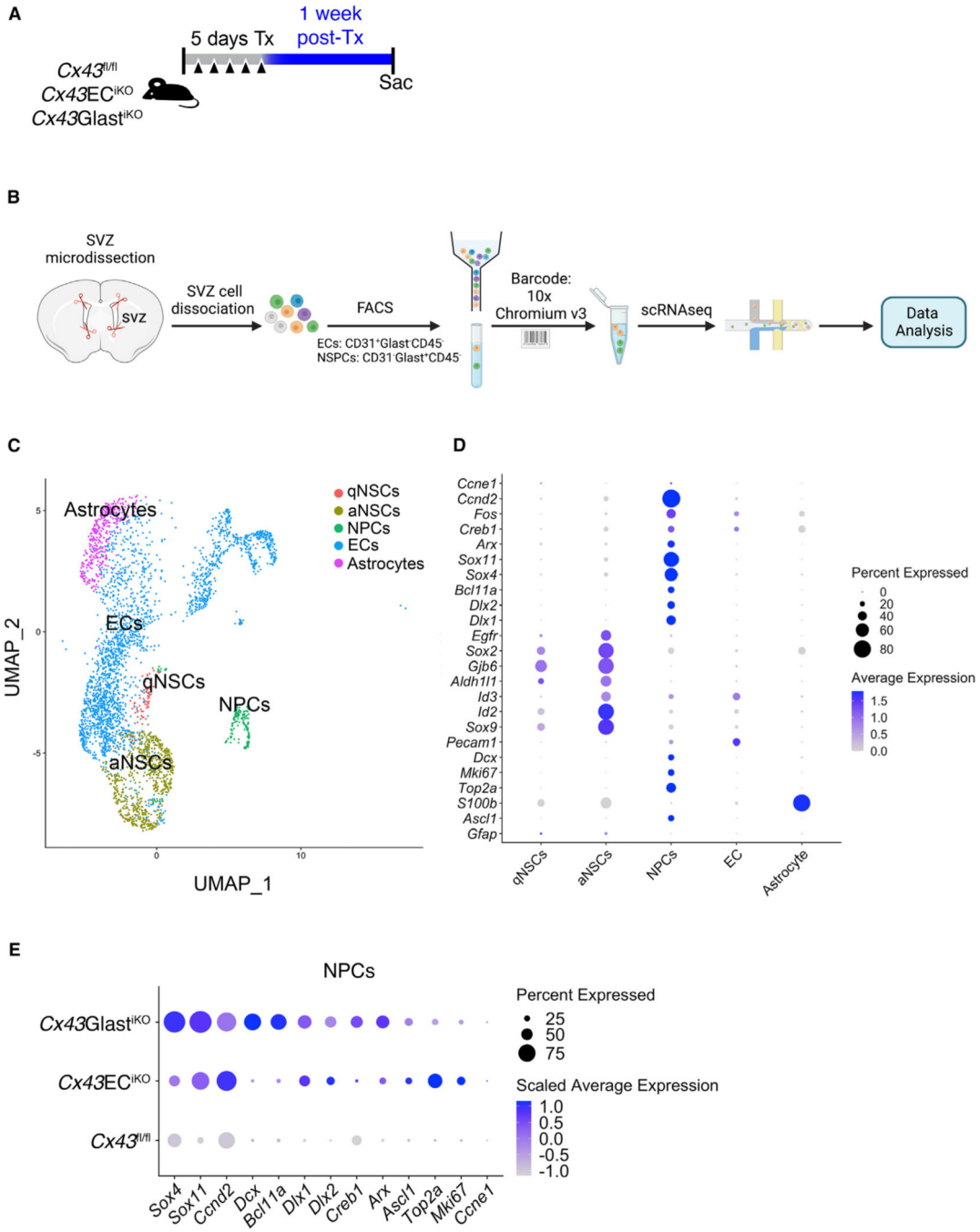

Figure 4. Single-cell RNA sequencing analysis of ECs and NSCs isolated from Cx43EC^{iKO} and Cx43Glast^{iKO} SVZs

(A) Timeline used to evaluate the effects of the short-term deletion of *Cx43* on the expression of genes regulating NSC behavior.

(B) Schematic of single cell isolation and single-cell RNA sequencing (scRNA-seq) protocol.

(C) Uniform manifold approximation and projection (UMAP) plot of scRNA-seq clustering with labeled cell types.

(D) Dot plot of cell type-specific marker expression in the clusters from (C).

(E) Dot-plot analysis displaying specific gene expression enriched for transit-amplifying progenitors and neuroblasts in the NPC clusters of *Cx43*$^{fl/fl}$, *Cx43*EC^{iKO}, and *Cx43*Glast^{iKO} mice.

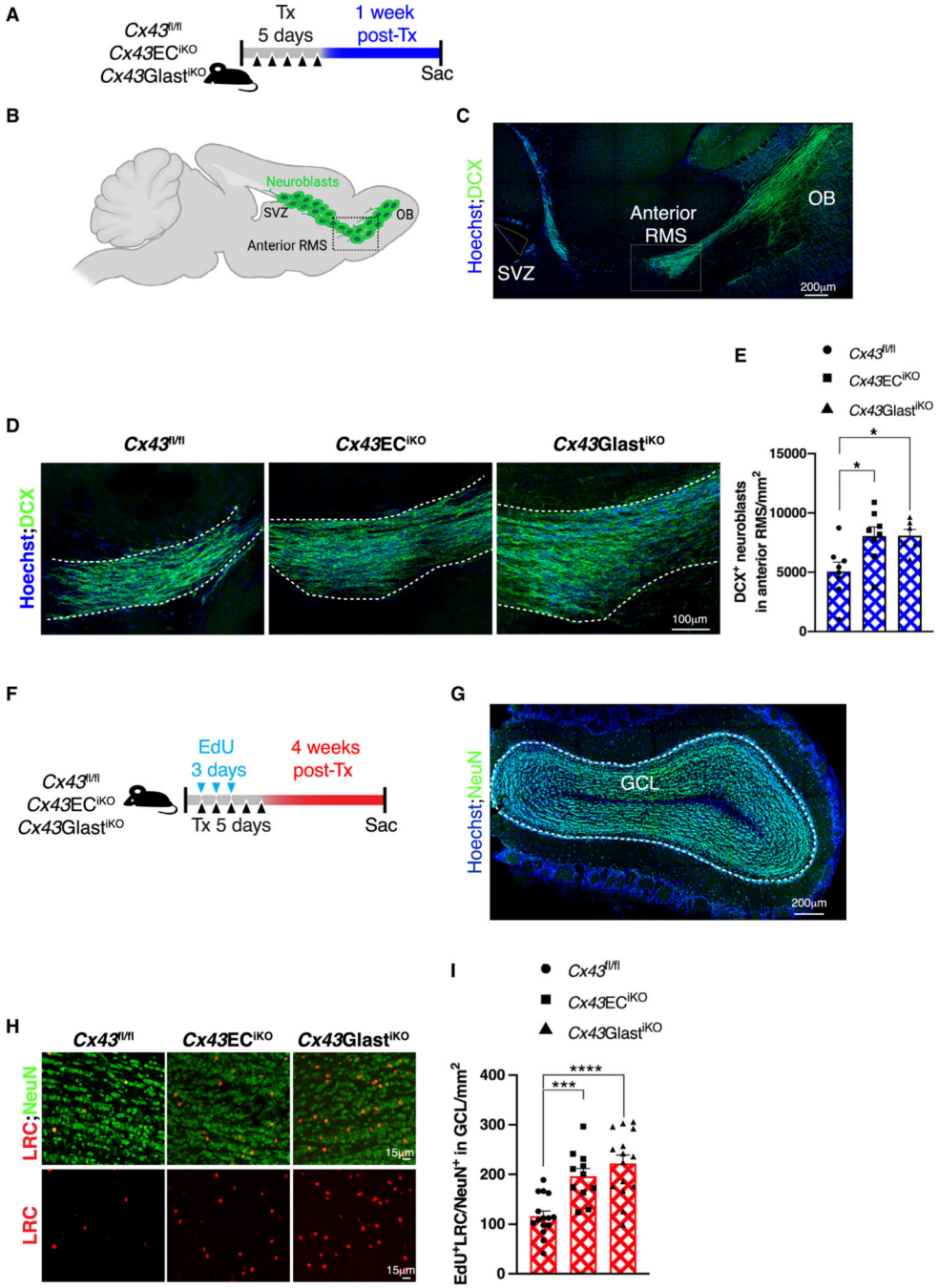

Figure 5. Cx43 deletion in ECs or NSCs increases neuroblasts in the RMS and neurogenesis in the OB

(A) Timeline used to evaluate the effects of the short-term deletion of *Cx43* on neuroblasts in the RMS.

(B) Schematic representation of a mouse brain sagittal section showing the RMS.

(C) Representative confocal image of DCX^+ neuroblasts in the RMS (50 μm section). Dashed boxes in (B) and (C) highlight the anterior RMS.

(D) Representative confocal images of DCX^+ neuroblasts in the anterior RMS (enclosed in white dashed lines) of *Cx43*$^{fl/fl}$, *Cx43*EC^{iKO}, and *Cx43*$Glast^{iKO}$ mice.

(E) Quantifications of images shown in (D) (n = 6–8 different sections analyzed from 3 animals per genotype).
(F) Timeline used to evaluate the effects of long-term deletion of *Cx43* on neurogenesis in the olfactory bulb.
(G) Representative confocal image of $NeuN^+$ newborn neurons (in green) on a coronal section (50 μm) of the mouse olfactory bulb. The dashed white lines outline the granule cell layer (GCL).
(H) Representative images of EdU^+ label-retaining cells (LRCs; red) and $NeuN^+$ newborn neurons (green) in GCL of $Cx43^{fl/fl}$, $Cx43EC^{iKO}$, and $Cx43Glast^{iKO}$ mice.
(I) Quantifications of images shown in (H) (n = 11–15 different sections analyzed from 3 different animals per group). Scale bars, 200 μm (C), 100 μm (D and G), and 15 μm (H). Data are mean ± SEM. *$p \leq 0.05$, ***$p \leq 0.001$, and ****$p \leq 0.0001$; analysis performed using the non-parametric Mann-Whitney statistical test. See also Figure S6.

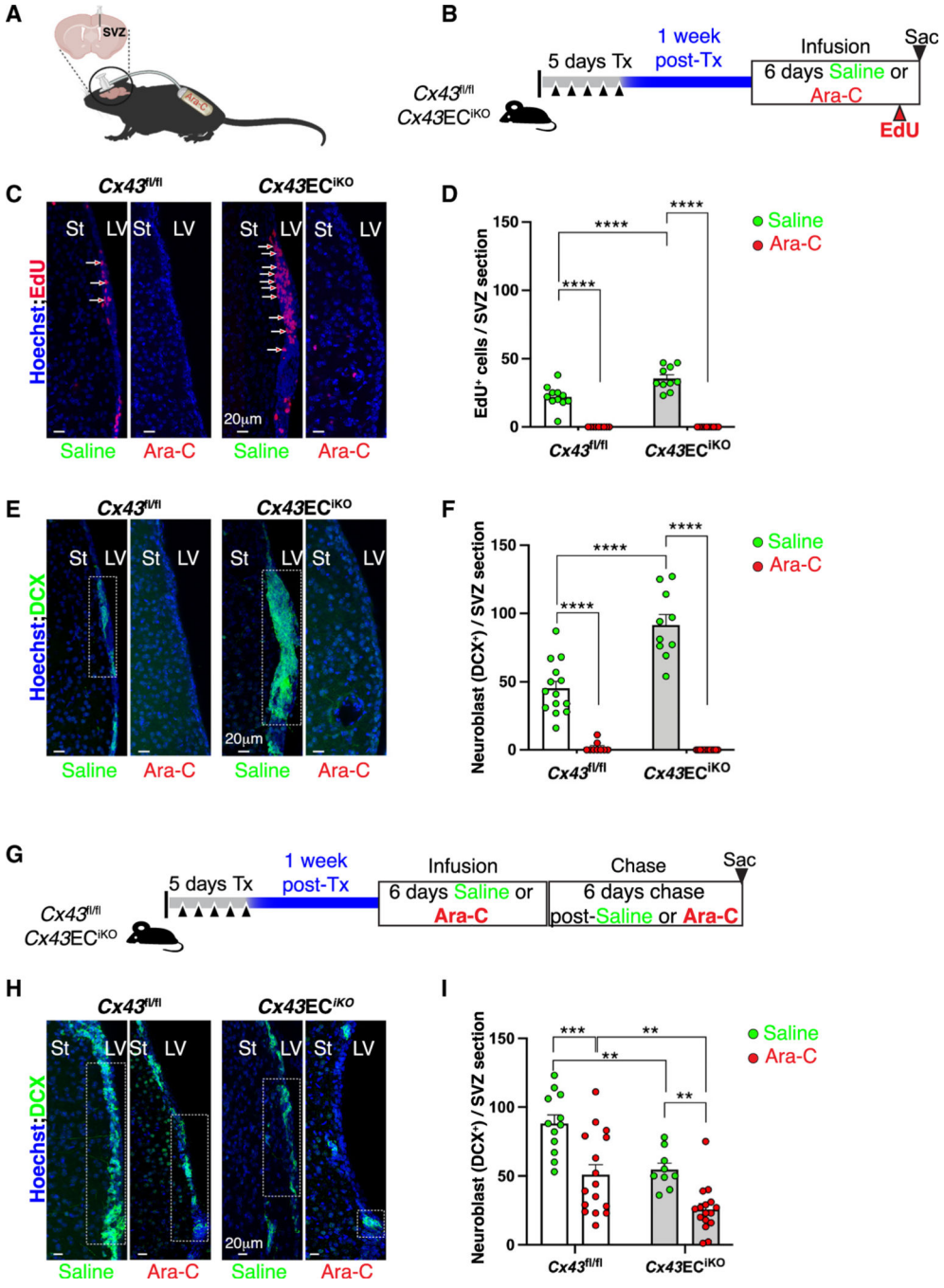

Figure 6. EC-expressed Cx43 is necessary for SVZ niche repopulation

(A) Schematic showing intraventricular brain infusion of Ara-C via an intra-cranial cannula connected to a subcutaneous micro-osmotic pump.

(B) Timeline used for saline or Ara-C infusions.

(C) Representative confocal images showing EdU^+ cells in SVZ section of saline vs. Ara-C infused *Cx43*$^{fl/fl}$ and *Cx43*EC^{iKO} mice after 6 days' infusion.

(D) Quantifications of images shown in (C) (n = 10–14 different SVZ sections analyzed from 3–5 different animals per group).

(E) Representative confocal images showing neuroblasts (DCX^+) in SVZ sections of saline vs. Ara-C infused *Cx43*$^{fl/fl}$ and *Cx43*EC^{iKO} mice.
(F) Quantifications of images shown in (E) (n = 12–14 different SVZ sections analyzed from 3–5 different mice per group).
(G) Timeline used for saline or Ara-C infusion and chase period.
(H) Representative confocal images showing neuroblasts (DCX^+) in SVZ of saline vs. Ara-C infused *Cx43*$^{fl/fl}$ and *Cx43*EC^{iKO} mice after infusions and chase period.
(I) Quantifications of SVZ sections shown in (G) (n = 9–16 SVZ sections analyzed from 3–5 different animals per group). Scale bar, 20 μm. St, striatum; LV, lateral ventricle.
Data are mean ± SEM. Two-way ANOVA with Šidák's multiple-comparison statistical tests was used for statistical analysis, and $p \leq 0.05$ was considered to indicate statistical significance. **$p \leq 0.01$, ***$p \leq 0.001$, and ****$p \leq 0.0001$. See also Figures S7 and S9.

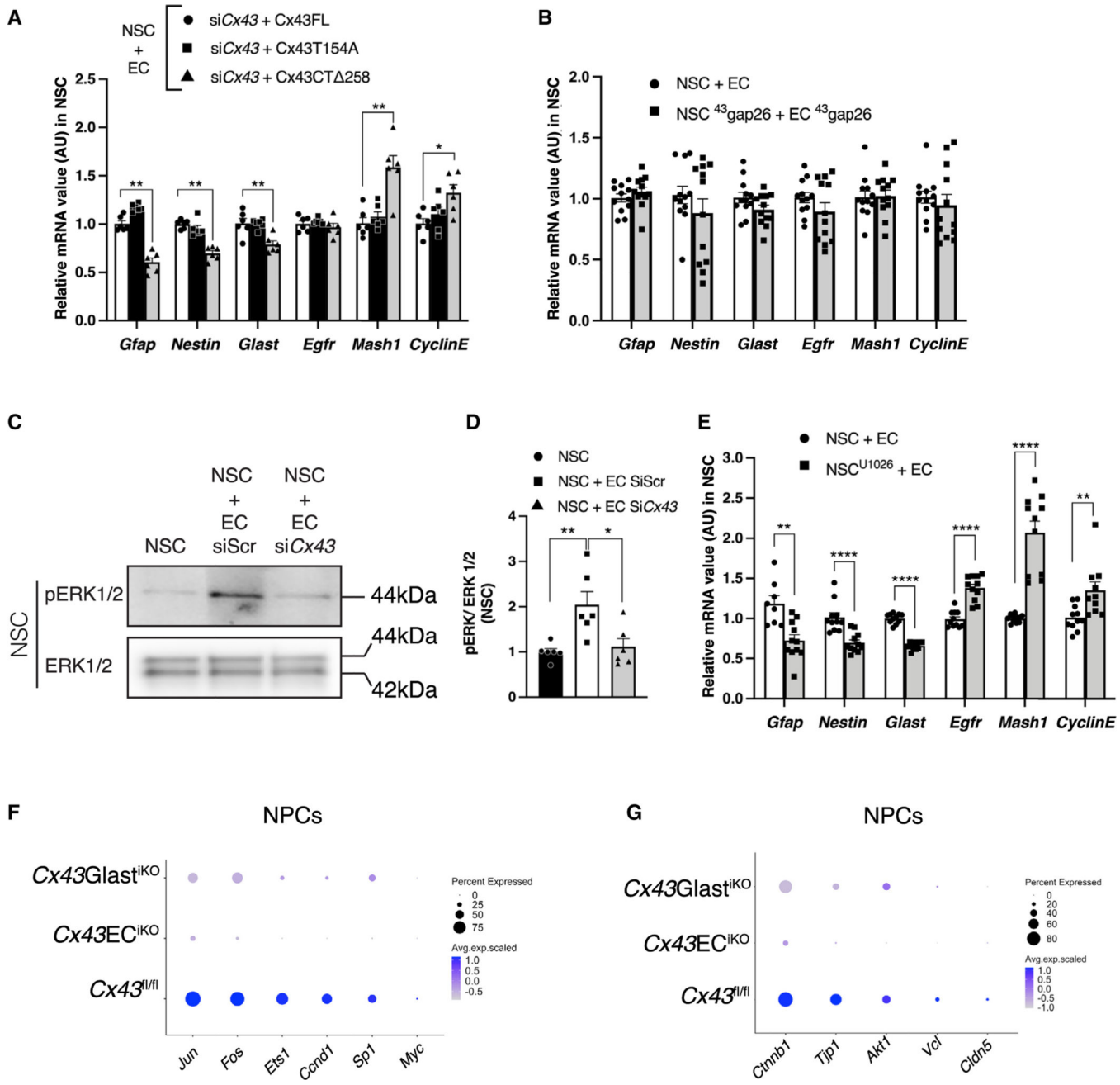

Figure 7. Cx43 cytoplasmic tail mediates EC-induced NSC quiescence in an ERK-dependent manner

(A) qPCR analysis of quiescent and activated genes in NSCs when co-cultured with ECs where both cell types are treated with Si*Cx43* followed by either the *Cx43*T154A mutant (Cx43 dead channel) or the *Cx43*CTΔ258 mutant (cytoplasmic tail truncated) compared with NSC-EC co-culture treated with Si*Cx43* followed by *Cx43* full length (FL) construct (n = 6 technical replicates from 3 different experiments).

(B) qPCR analysis of quiescent and activated genes in NSCs when co-cultured with ECs where both cell types are treated with ^{43}gap 26 compared with NSC-EC co-culture (n = 12 technical replicates from 4 different experiments).

(C and D) Western blot analysis of pERK and ERK protein levels in NSCs cultured alone or co-cultured with ECs treated with control siRNA (SiScr) or *Cx43* siRNA (Si*Cx43*) (C); quantifications are shown in (D) (n = 6 biological replicates).

(E) qPCR analysis of qNSCs and aNSCs co-cultured with ECs where NSCs is treated with the ERK signaling inhibitor U0126 compared with NSCs and ECs co-culture (n = 11 technical replicates from 3 different experiments).

(F) Dot-plot analysis displaying specific gene expression of ERK activation pathway in the NPC clusters of *Cx43*$^{fl/fl}$, *Cx43*EC^{iKO}, and *Cx43*Glast^{iKO} mice.

(G) Dot-plot analysis displaying specific gene expression of Cx43 cytoplasmic tail interaction partners in the NPC clusters of *Cx43*$^{fl/fl}$, *Cx43*EC^{iKO}, and *Cx43*Glast^{iKO} mice.

Data are mean ± SEM. *p ≤ 0.05, **p ≤ 0.01, ***p ≤ 0.001, and ****p ≤ 0.0001; analysis performed using the non-parametric Mann-Whitney statistical test. See also Figure S8.

KEY RESOURCES TABLE

REAGENT or RESOURCE	SOURCE	IDENTIFIER
Antibodies		
Rabbit anti-Connexin 43 (1:1000 for IF or 1:500 for Western Blot)	Abcam	Cat# ab11370; RRID: AB_297976
Rat anti-SOX2 (1:100)	ThermoFisher	Cat# 14-9811-82; RRID: AB_11219471
Rabbit anti-EGFR (1:75)	Millipore	Cat# 06-847; RRID_AB_2096607
Rabbit anti-Doublecortin (1:200)	Abcam	Cat# ab18723; RRID: AB_732011
Chicken anti-Doublecortin (1:200)	AVES Lab	Cat# DCX; RRID: AB_2313540
Rabbit anti-GFAP (1:400)	Agilent	Cat# Z0334; RRID: AB_10013382
Chicken anti-GFAP (1:400)	AVES Lab	Cat# GFAP; RRID: AB_2313547
Hamster anti-PECAM1 (1:100)	Millipore	Cat# MAB1398Z; RRID: AB_94207
Rabbit anti-NeuN (1:500)	Abcam	Cat# ab104225; RRID: AB_10711153
Rabbit anti- S100β (1:300) (1:300)	Agilent	Cat# Z0311; RRID: AB_10013383
Rabbit anti-CASPASE 3 (1:200)	Cell Signaling	Cat# 9661S; RRID: AB_2341188
Rabbit anti-phospho p44/42 MAP kinase (pERK1/2, 1:1000)	Cell Signaling	Cat# 9106; RRID: AB_331768
Rabbit anti-p44/42 MAP kinase (ERK1/2, 1:1000)	Cell Signaling	Cat# 9102; RRID: AB_330744
Chicken anti-GFP (1:500)	Abcam	Cat# ab13970; RRID: AB_300798
Rabbit IgG anti-Glast-FITC	Alomone	Cat# AGC-021-F
Rat IgG_{2a} anti-CD31-PE	Pharmingen™	Cat# 553373
Rat IgG_{2b} anti-CD45-V450	Pharmingen™	Cat# 560501
Chemicals peptides and recombinant proteins		

REAGENT or RESOURCE	SOURCE	IDENTIFIER
U1026	Cell Signaling	Cat# 9903S
43gap26	Genscript	Cat# RP20274
Corn oil	Sigma	Cat# C8267
Cultrex Laminin	R&D Systems	Cat# 3446-005-01
Cytosine-β-arabinofuranoside	Sigma	Cat# CC6645
EdU	Thermo Fisher	Cat# A10044
Heparin	Sigma	Cat# H3149-250KU
Recombinant human FGF	Preprotech	Cat# 100-18B
Recombinant murine EGF	Preprotech	Cat# 315-09
Tamoxifen	Sigma	Cat# T5648-1G
DAKO mounting media	Agilent DAKO	Cat# S3023
HRP substrate Radiance plus	Azure Biosystems	Cat# AC2103
RIPA	Abcam	Cat# ab206996
Paraformaldehyde	Sigma	Cat# 252549
DMEM/F12	Sigma	Cat# D8437
Glucose	Sigma	Cat# G8644
Percoll	Sigma	Cat# P1644
Vascupaint™	ediLumine	SKU MDL-122
Critical commercial assays		
EdU Click-iT™	Invitrogen	Cat# C10337
RNeasy Plus Micro Kit	Qiagen	Cat# 74034
cDNA Reverse Transcription Kit	Thermo Fisher	Cat# 4368813
PowerUp SYBR green Master Mix	Thermo Fisher	Cat# A25778
Lipofectamine RNAimax	Thermo Fisher	Cat# 13778030
Pierce™ BCA™ Assay kit	Thermo Fisher	Cat# 23252
Deposited data		
Single cell RNAseq data of SVZ populations	This paper	GEO: GSE221558
Experimental models: Cell lines		

REAGENT or RESOURCE	SOURCE	IDENTIFIER
Mouse ANS4-GFP	Gift from S. Pollard, University of Edinburgh, (Pollard et al.)[30]	N/A
Mouse bEnd.3	ATCC	Cat# CRL-2299™; RRID: CVCL_0170
Experimental models: Organisms/strains		
*Cdh5*Cre^{ERT2}1Rha	Gift from Ralf Adam's laboratory (Sorensen et al.[67]; Wang et al.)[68]	N/A
*Slc1a3*Cre^{ERT2}	Gift from Jean Léon Thomas laboratory, Yale University	N/A
Gja1^{tm1Dlg} or Cx43^{flox}	Jackson Laboratory	Strain# 008039; RRID: IMSR_JAX:008039
ROSA$^{mT/mG}$	Jackson Laboratory	Strain# 007676; RRID: IMSR_JAX:007676
Oligonucleotides		
PCR genotyping primers sequences	W.M. Keck Laboratory, Yale University	Table S1
qPCR primers sequences	W.M. Keck Laboratory, Yale University	Table S2
Cx43 primers sequences	GenScript Eurofin	Table S3
Cx43 siRNA Smartpool	Dharmacon	Cat# L-051694-00-0005
Recombinant DNA		
GJA1 cDNA	GenScript	Cat# NM_010288.3
pTRE-TIGHT-Cx43-eYFP	Gift from Robin Shaw	Addgene plasmid# 31807; RRID: Addgene_31807
pcDNA3.1-HA	Gift from Oskar Laur	Addgene plasmid# 128034; RRID: Addgene_128034
Software and algorithms		
Graphpad Prism 8	Graphpad Prism Inc	RRID:SCR_002798
ImageJ v1.53a	NIH	RRID: SCR_003070
Adobe Illustrator	Adobe	RRID: SCR_010279
Adobe Photoshop	Adobe	RRID: SCR_014199
BioRender	http://biorender.com	RRID:SCR_018361
Seurat 4.2	Satija Laboratory	https://www.satijalab.org/seurat
Galaxy ToolShed v 1.0.2	N/A	http://hannonlab.cshl.edu/fastx_toolkit/

REAGENT or RESOURCE	SOURCE	IDENTIFIER
Other		
Digital Image Analyzer	Azure Imager	Cat# C300
DMi8 LIGHTNING® confocal microscope	Leica	Cat# SP8
BD FACS sorter	BD	Cat# Melody
Fast-Real Time PCR machine	Applied Biosystems	Cat# QuantStudio Flex6
Leica Vibratome	Leica	Cat# VT1000S
Micro-osmotic pump	Alzet®	Cat# 1007D